SPACE RESEARCH COORDINATION CENTER

A MATHEMATICAL STUDY OF THE ELECTRON DECAY IN DIFFUSION AND RECOMBINATION CONTROLLED AFTERGLOWS

BY

LOTHAR FROMMHOLD AND

MANFRED A. BIONDI

DEPARTMENT OF PHYSICS

SRCC REPORT NO. 71

UNIVERSITY OF PITTSBURGH

PITTSBURGH, PENNSYLVANIA

26 FEBRUARY 1968

APP. 16

A Mathematical Study of the Electron Decay In Diffusion and Recombination Controlled Afterglows

Lothar Frommhold and Manfred A. Biondi

(Annals of Physics)

University of Pittsburgh

Pittsburgh, Pennsylvania

February 1968

A Mathematical Study of the Electron Decay In Diffusion and Recombination Controlled Afterglows*

Lothar Frommhold, (University of Texas), and Manfred A. Biondi, (University of Pittsburgh)

Abstract: The continuity equation for electrons in a decaying plasma is solved numerically in three dimensions including a loss term quadratic in the electron density (i.e. two-body electron-ion recombination) and an ambipolar diffusion term. The geometries investigated are the finite cylinder, the rectangular parallelepiped and some one-dimensional cases. The electron densities are averaged assuming weighting functions corresponding to various microwave probing field distributions (cylindrical TM_{010}, TE_{011} and TE_{111} and retangular TE_{101} modes) and are therefore directly proportional to measured quantities, such as resonant frequency shifts, obtained in microwave afterglow studies of recombination. Three different initial electron distributions are used, corresponding to a uniform (recombination controlled), a fundamental mode diffusion, and a somewhat more spatially con~~re~~stricted distribution. The linear range of the computed reciprocal of the (averaged densities)$^{-1}$ versus time curves is determined and correction factors are derived which, if applied to the observations, yield the corrected recombination coefficients from the curves. The corrections derived in the two- and three-dimensional analyses are found to be significantly larger than those obtained in the one-dimensional analyses. Also, when considering

*This research was supported, in part, by the Defense Atomic Support Agency and the Army Research Office (Durham), DA-31-124-ARO(D)-G-518.

plasma containers of different shapes but of the same fundamental diffusion length, a larger surface/volume ratio is found to be equivalent in effect to an increased diffusion coefficient in the predicted decays. In most cases of practical interest, though, a much stronger dependence upon the varying probing field distributions is found when different container or dimensions are to be compared. When the present analysis is applied to one-dimensional geometries, recombination corrections in agreement with the results of Gray and Kerr are obtained.

I. Introduction

Some of the principal methods of studying electron-ion recombination involve determinations of the rate of decay of electron density from an initially ionized gas, i.e. afterglow studies. The interaction of free electrons in an ionized gas (plasma) with a microwave probing field provides a convenient method for determining the average electron concentration during the afterglow. It has been shown [1] that the electron current density $\underset{\sim}{J}$ which flows at a given point in space in response to an applied field $\underset{\sim}{E}$ of angular frequency ω is,

$$\underset{\sim}{J} = \sigma_c \underset{\sim}{E} = (ne^2/[m(\nu_c + i\omega)]) \cdot \underset{\sim}{E} \quad , \qquad (1)$$

where σ_c, the complex conductivity, is given by the term in parentheses on the right for the case of a collision frequency, ν_c, which does not depend on electron energy; n, e, and m are electron density, charge and mass, respectively.

In general, the various microwave cavity and waveguide propagation techniques [2,3,4,5] measure the real and/or imaginary parts of $(\underset{\sim}{J} \cdot \underset{\sim}{E})$. For example, according to perturbation theory [6], the change in Q and the resonant frequency shift, ΔF_o, of a microwave cavity containing a conducting medium is given by

$$\left(\frac{1}{Q_o} - \frac{1}{Q_{oe}}\right) - \frac{2i\Delta F_o}{F_{oe}} \simeq \frac{1}{\epsilon_o \omega_{oe}} \cdot \frac{\int_{cav} \underset{\sim}{J} \cdot \underset{\sim}{E}\, d^3r}{\int_{cav} E^2\, d^3r} \quad , \qquad (2)$$

where the subscripts o and oe refer to the cavity, respectively, with and without the ionized gas, and ϵ_o is the permittivity of free space. Thus,

$$\frac{\Delta F_o}{F_{oe}} \simeq \left[\frac{e^2}{2 m \epsilon_o (\omega_{oe}^2 + \nu_c^2)} \right] \cdot \frac{\int_{cav} n(\underset{\sim}{r}) E^2(\underset{\sim}{r}) d^3 r}{\int_{cav} E^2(\underset{\sim}{r}) d^3 r} \qquad (3)$$

The integral in the numerator is non-zero only in that part of the cavity occupied by plasma and could therefore have been restricted to that volume.

If we introduce a "microwave-averaged" electron density, [6]

$$\bar{n}_{\mu w} \equiv \int_{cav} n(\underset{\sim}{r}) E^2(\underset{\sim}{r}) d^3 \underset{\sim}{r} \Big/ \int_{cav} E^2(\underset{\sim}{r}) d^3 r = C \Delta F_o \qquad (4)$$

we see from eq. (3) that this form of averaged electron density is directly related to the measured frequency shift by the coefficient

$$C = \frac{4 \pi m \epsilon_o (\omega_{oe}^2 + \nu_c^2)}{\omega_{oe} e^2} , \qquad (5)$$

without making assumptions concerning the spatial form of $n(\underset{\sim}{r})$. This point is discussed further in Sec. II.

In order to obtain quantitative determinations of electron-ion recombination rates from the observed decay of the average electron density (inferred from such measurements as cavity frequency shift), it is necessary to solve the electron continuity equation for $n(\underset{\sim}{r}, t)$ and from this to form the appro-

priate average, such as $\bar{n}_{\mu w}(t)$, to compare with the measured values. In practice, this has rarely been done. Instead, unrealistic assumptions have been made to simplify the analysis (i.e. that the electrons maintain a uniform distribution in the container throughout the afterglow) or appeal is made to correction factors derived by Gray and Kerr [7] from computer solutions of the electron continuity equation for one-dimensional (infinite cylinder, sphere) configurations.

The present paper extends the work of Gray and Kerr to numerical solutions of the recombination and diffusion controlled electron continuity equation in more realistic, three-dimensional configurations (finite cylinders, rectangular parallelepipeds). From these solutions, correction factors for various plasma container and microwave probing field geometries are derived.

II. Electron Continuity Equation

We assume that the electron energy distribution has reached a stationary form in the afterglow, so that it is only necessary to consider the coordinate space electron continuity equation. On the assumption that electron production terms are negligible and that the only significant volume electron loss is recombination, the continuity equation becomes

$$\frac{\partial n}{\partial t} \simeq D_a \nabla^2 n - \alpha n^2 \qquad (6)$$

where D_a is the ambipolar diffusion coefficient and α is the rate coefficient of a two-body recombination process, such as dissociative recombination. In this form, it is assumed a) that there is only one species of positive ion and no negative ions, and b) therefore, as a result of quasi-neutrality of a plasma, the

densities of electrons and positive ions are essentially equal, and c) that the Debye length is always much smaller than the container dimensions, so that ambipolar diffusion holds throughout the afterglow period under consideration. In an analysis of this type, other production and loss terms can be (and have been) included, for example, metastable ionization and electron attachment to neutrals; however, a discussion of the resulting solutions of the continuity equation is beyond the scope of the present paper.

The boundary condition $n = 0$ at the walls of the container has been applied and several different initial electron distributions, as described in Sec. III b, were used. By means of a numerical integration scheme (see Sec. III c) a solution of eq. (6) with its initial and boundary conditions, is obtained. Thus, mean densities according to eq. (4) can be evaluated for various modes of the probing field $E^2(\underset{\sim}{r})$. The time variation of the computed average $\bar{n}_{\mu w}$ is then obtained for various values of the recombination and ambipolar diffusion coefficients, α and D_a .

In order to provide correction factors for use in recombination studies which do not employ the detailed solutions of eq. (6) together with computations of $\bar{n}_{\mu w}$ through eq. (4), we proceed as follows. If one neglects the diffusion term in eq. (8), the well-known "recombination solution".

$$1/n\,(\underset{\sim}{r},t) = \left[1/n\,(\underset{\sim}{r},o)\right] + \alpha t \quad , \qquad (7)$$

where $n\,(\underset{\sim}{r}, o)$ is the initial electron distribution at t=o, results. In many studies it has been customary to assume that the electrons maintain a uniform distribution throughout the plasma container during the afterglow. Thus, from eq. (7), the decay of this uniformly distributed electron density, n_u, is

given by

$$1/n_u(t) = 1/n_u(o) + \alpha t \tag{8}$$

It has been shown [7,8,9] that the identification of the slope of a $1/n_u$ vs t plot as the desired recombination coefficient is substantially in error when actual electron spatial distributions are considered.

The method of quantitatively correcting such data to find α involves introduction of an alternative "microwave averaged" electron density,

$$\bar{n}(t) = \int_{\text{plasma vol}} n(\underset{\sim}{r}, t)\, E^2(\underset{\sim}{r})\, d^3r \Big/ \int_{\text{plasma vol}} E^2(\underset{\sim}{r})\, d^3r = C'\Delta F_o \tag{9}$$

where by restricting the integrals to the plasma volume, we have a quantity $\bar{n}(t)$ which reduces to $n_u(t)$ if we assume the electrons to be uniformly distributed throughout the plasma. Again, $\bar{n}(t)$ is directly related to the measured frequency shifts by the coefficient $C' = CG$, see eq. (5), where G is the geometry factor

$$G = \int_{\text{cavity}} E^2(\underset{\sim}{r})\, d^3\underset{\sim}{r} \Big/ \int_{\text{plasma vol}} E^2(\underset{\sim}{r})\, d^3\underset{\sim}{r} \tag{10}$$

By these definitions, we have introduced a quantity, $\bar{n}(t)$, which is readily obtained from the computed $n(\underset{\sim}{r}, t)$ values and is equivalent to the quantity which is often used for presenting the experimental data in recombination analyses. We have also provided for the often-encountered experimental condition of a plasma which is restricted to less than the full microwave cavity volume. For some useful expressions of G in terms of the container

and cavity dimensions, see the appendix.*

Although the solution of the continuity equation, eq. (6), including the diffusion term,can not be expected to follow the form of eq. (8) throughout the afterglow, it is found that there are ranges of $1/\bar{n}$ (t) values for which an approximately linear increase of $1/\bar{n}$ with afterglow time is observed. Thus over a certain time interval we may represent the observed electron density decay by a straight line,

$$1/\bar{n}\,(t) = 1/\bar{n}\,(0) + a\,t \tag{11}$$

where the slope a is to be related by appropriate factors to the desired recombination coefficient, α. If we define the "linear range" of eq. (11) as the ratio f between the largest and smallest values of $1/\bar{n}$ (t) for which the data points or computed curves lie sufficiently close to the best-fitting straight line, on a $1/n$ vs t plot, then the necessary correction factor Δ between a and α, defined by,

$$\alpha \equiv a\,(1 - \Delta) \tag{12}$$

is directly related to the value of f, i.e., $\Delta \equiv \Delta\,(f)$. The correction factor Δ also depends on plasma container and cavity shapes and dimensions, on the microwave probing field distribution and on the initial electron spatial distribution.

---

* It should be noted that G depends not solely upon the geometries; it is somewhat dependent on the field distributions, too.

III Method of Obtaining Correction Factors

We wish to obtain values of the correction factor, Δ, for the wide variety of experimental conditions that are encountered in the various recombination studies. In what follows we shall adopt the pattern set by Gray and Kerr [7]. In particular, we shall use their terminology and mathematical formulation (though not their integration method) of the problem, which we briefly review here. Eq. (6) is replaced by a "normalized" equation, in which the variables and functions are dimensionless.

$$\frac{\partial N}{\partial \tau} = \nabla^2 N - \beta N^2 \tag{13}$$

where

$$\beta = (\alpha n_o) \Big/ (D_a / \Lambda^2) \tag{14}$$

The normalized density $N = n/n_o$ is obtained by dividing the actual densities $n = n(\underset{\sim}{r}, t)$ by the initial central density n_o. The normalized time variable $\tau = (D_a / \Lambda^2) \cdot t$ is proportional to the real time t, the coefficient of proportionality being the ambipolar diffusion coefficient divided by the square of the fundamental diffusion length (see Sec. III f). The normalized cartesian ξ, η, ζ, and cylindrical coordinates ρ and ζ, respectively, are obtained by dividing the respective spatial variables x,y,z, r and z, by Λ. The "normalized" recombination coefficient β is proportional to α, eq. (14). The boundary and initial conditions for the normalized density N are simply that N=0 at the walls and that the initial value be 1 at the center of the container, $N(\underset{\sim}{0},0)=1$.

In our work two and three-dimensional "normalized" Laplaceians for rectangular and cylindrical geometries are used, i.e.,

$$\nabla^2 = \frac{\partial^2}{\partial \rho^2} + \frac{1}{\rho}\frac{\partial}{\partial \rho} + \frac{\partial^2}{\partial \zeta^2} \qquad (15)$$

and

$$\nabla^2 = \frac{\partial^2}{\partial \xi^2} + \frac{\partial^2}{\partial \eta^2} + \frac{\partial^2}{\partial \zeta^2} \qquad (16)$$

We have also used one-dimensional normalized Laplacians for infinite parallel planes, for the infinite cylinder, and for the sphere. In this way we are able to compare our results with previous solutions of the continuity equation. (7,8,)

a) Surface-to-volume ratio. Because of the enlarged number of parameters in two- and three-dimensional solutions of the continuity equation, we seek those parameters which permit the correction factors calculated for a limited number of plasma container shapes and probing field distributions to be applied, with reasonable accuracy, to other cases. One such parameter is the ratio of the surface A and the volume V of a plasma container, which we introduce in normalized form by multiplying by the fundamental diffusion length Λ, i.e.,

$$g \equiv (A/V)\,\Lambda. \qquad (17)$$

Physically, this is an important parameter, since the electron loss by recombination occurs throughout the volume of the container, while ambipolar diffusion loss to the boundaries depends on the surface area of the container.

It is a straightforward matter to show that, for a finite cylinder of normalized dimensions ρ_o and ζ_o, $g = 2\cdot\left[(1/\rho_o) + (1/\zeta_o)\right]$ and for a rectangular parallelepiped (ξ_o, η_o, ζ_o), $g = 2\cdot\left[(1/\xi_o) + (1/\eta_o) + (1/\zeta_o)\right]$.

For the "one-dimensional" geometries; we find, $g = 2/\pi$ for infinite parallel planes, $g = 2/(2.405)$ for infinite cylinder, and $g = 3/\pi$ for the sphere. Thus, for essentially all of the geometries employed in recombination studies to date g-values lying between 0.64 (parallel planes) and 1.10 (cube) are encountered. It is of interest to note that different container geometries may have equal g- values. For example, there is a variety of finite cylinders and parallelepipeds having the same g- values as spheres or the infinite cylinder, see figure 1.

b) Initial density distributions. In order to integrate eq. (6) or eq. (13), we require an initial condition - the electrons' spatial distribution at t = o. Experimentally such initial distributions have been crudely determined, at best, by such techniques as observation of the spatial distribution of the spatial distribution of the radiation accompanying the recombination process [9, 10]. In order to embrace the variety of initial distributions encountered in practice, we have used the fundamental mode diffusion distribution raised to the $0^{\underline{th}}$, $1^{\underline{st}}$ and $2^{\underline{nd}}$ powers. Thus, for a finite cylinder, initial distributions of the form

$$N(r, z, o) = \left[J_o (2.4\, r/r_o) \cdot \cos (\pi\, z/z_o) \right]^k \tag{18}$$

and for a rectangular parallelepiped

$$N(x, y, z, o) = \left[\cos (\pi x / x_o) \cdot \cos (\pi y / yo) \cdot \cos (\pi z/z_o) \right]^k \tag{19}$$

are used. For k = o we have the uniform "recombination controlled" distribution, for the "squared diffusion distribution", which is a plasma approximating the "plasma ball" mode of discharge sometimes noted at higher gas

pressures. In practice, observations of the spatial distribution of recombination radiation and comperisons between computed and observed electron decays in neon [10, 11] have indicated that k values lying between 1 and 2 best approximate practical initial distributions.

c) Computer Solution Method. The several sections of the computer program are briefly reviewed here. In one section, the differential equation (13) is solved by replacing the time derivative by the (crude) "forward difference quotient"

$$\partial N/\partial \tau \rightarrow \left[N\Big|_{(\tau + \Delta\tau)} - N\Big|_{\tau} \right] / \Delta\tau \qquad (20)$$

which has been reported [12] to be a much better substitution than other expressions of a higher approximation, for parabolic equations. The spatial derivatives are replaced by the second order expressions

$$\partial N/\partial \rho \rightarrow \left[N\Big|_{(\rho+\Delta\rho)} - N\Big|_{(\rho-\Delta\rho)} \right] / 2\Delta\rho \qquad (21)$$

and

$$\partial^2 N/\partial \rho^2 \rightarrow \left[N\Big|_{(\rho + \Delta\rho)} - 2N\Big|_{\rho} + N\Big|_{(\rho - \Delta\rho)} \right] / (\Delta\rho)^2. \qquad (22)$$

Similar expressions are taken for the derivatives with respect to ξ , η , ζ . In this way, a very simple, explicit formula for "new" density values at the time $(\tau + \Delta\tau)$ is obtained from the knowledge of all density values at the time τ. This formulation is well-behaved in the computation, if the temporal increment $\Delta\tau$ does not exceed the limit, $\Delta\tau_{max}$, given by

$$\Delta\tau \leq \tau_{max} = \{ 2\cdot[(1/\Delta\xi)^2 + (1/\Delta\eta)^2 + (1/\Delta\zeta)^2]\}^{-1} \qquad (23)$$

and

$$\Delta\tau \leq \Delta\tau_{max} = \{ 2[(1/\Delta\rho)^2 + (1/\Delta\zeta)^2] \}^{-1} \qquad (24)$$

for finite cylinders and parallelepipeds, respectively. The quantities $\Delta\xi$, $\Delta\eta$, $\Delta\zeta$ and $\Delta\rho$ designate meshwidths in the ξ, η, ζ and ρ directions. In our computations, the condition eq. (23) or (24) has always been met. Thus, the solution of our difference equation converges to the solution of the differential eq. (13) as the mesh is refined [12, 13]. At the same time, application of this condition produced a favourable behaviour of our computation scheme with regard to the propagation of errors, such as truncation errors[12].

The selected time increment $\Delta\tau$ is computed anew at the start of each cycle. Initially, the recombination term $-\beta N^2$ in eq. (13) is much more important than the diffusion term $\nabla^2 N$, and time increments are needed which are a small fraction of the upper limit, eq. (23) or (24). In this case $\Delta\tau$ is chosen so that the ~~temporal~~ decrease of N at the center is a small fraction (usally 1%) of the center density at that time. However, as this process is continued, with increasing time N decreases and the quadratic term becomes less and less important. The $\Delta\tau$ values thus computed finally become larger than the limit. In this case, $\Delta\tau$ is set equal to the limit given by eq. (23) or eq. (24).

When the density values at all spatial mesh points have been obtained at a given time τ, the average, eq. (9), is computed and recorded and, by means of an interpolation programme, the function $1/\bar{N}$ versus τ is evaluated at equidistant time intervals. Finally, a straight line $Y = Y_0 + S\tau$ is

sought to optimally fit the linear portion of the function $1/\overline{N}$, as suggested in the discussion of eq. (11). We used Tshebysheff polynomials and a least mean square curve fitting method[14]. An upper and a lower time limit, τ_u and τ_ℓ , are then found such that the $1/\overline{N}$ curve deviates by ϵ from the straight line. ϵ was set equal to 2% of the arithmetic average of the upper and lower reciprocal density values

$$\epsilon = 0.02 \cdot \{ 1/\overline{N}(\tau_u) + 1/\overline{N}(\tau_\ell) \} / 2 \tag{25}$$

The part of the $1/\overline{N}$ versus τ curve between τ_ℓ and τ_u is called the "linear portion" of this curve. The linear range f introduced earlier may be defined as

$$f \equiv \overline{N}(\tau_\ell) / \overline{N}(\tau_u) \tag{26}$$

and the correction factor Δ introduced in eq. (12) expressed in terms of normalized quantities,

$$\Delta \equiv (S - \beta)/S = (a - \alpha)/a \tag{27}$$

From the computations, both f and Δ have been calculated as functions of the parameter β . These data are presented in figs. 2 through 7 and 9 through 22.

Since different straight lines can be found for different portions of one calculated $1/\overline{N}$ vs τ curve, we used a program to select, from among the many straight lines, that line which gave a maximum f value in following the curve. For larger β values (>20) , one particular straight line clearly

exhibited maximum f value, so that in these cases, the f and Δ values selected are uniquely determined. For smaller β's, when occasionally several or many "optimal" straight lines were found with almost constant f's, the particular one embracing the earliest afterglow interval was chosen. All other ones exhibited larger correction factors Δ. It should also be noted that, in the majority of the computed cases, the $1/\overline{N}$ vs τ curves exhibited sufficiently small initial departures from straight lines that τ_ℓ was equal to zero time.

d) Microwave Probing Field Modes. An additional objective of this investigation is to study the effect of various microwave field weighting functions, E^2, in the evaluation of the averaged density, eq. (9). For cylindrical plasma containers we have considered cylindrical cavities excited in the TM_{010}, TE_{111}, and TE_{011} modes.[15]. The corresponding weighting functions are, $E^2 = [J_o(2.4\, r/r_1)]^2$ for the TM_{010} mode, $E^2 = \{\alpha^{-2}J_1^2(\alpha) + J_1'^2(\alpha)\}\cos^2(\pi z/z_1)$, where $\alpha = 1.84\, r/r_1$ for the TE_{111} mode, and $E^2 = [J_1(3.83\, r/r_1)\cdot\cos(\pi z/z_1)]^2$ for the TE_{011} mode. (The subscript 1 indicates cavity dimensions.) We note that, for a TM_{010} mode, the field E^2 is a maximum at r = 0 and falls monotonically to zero as r approaches the cavity radius r_1. There is no z- dependence of the field, thus the field at the flat end walls of the cylinder is non-vanishing. For a TE_{111} mode, we have a maximum field in the center, with monotonically falling field strengths toward the walls in both the r and z directions. For this mode, the field vanishes at the flat end walls, but not at the clyindrical walls. The TE_{011} mode has the same z-dependence as TE_{111} but E^2 is zero everywhere on the center line, increases initially with increasing r and finally decreases to zero as r approaches r_1.

For rectangular parallelepipeds, a TE_{101} mode is used with a corresponding weighting function, $E^2=[\cos(\pi y/y_1).\cos(\pi z/z_1)]^2$. The weighting function is constant in the x-direction, with non-vanishing fields at the walls perpendicular to the x-axis. In the y and z directions, the field falls monotonically to zero at the walls.

It is clear that different weighting functions emphasize different regions of the plasma in terms of their effect on the frequency shift, ΔF_o. The cylindrical TM_{010} mode de-emphasizes, for example, a sheath in the vincinity of the cylindrical walls (and thus is the ideal mode for long cylinders). However, the regions near the end walls are important. Conversely, for cylindrical TE_{111} modes, these end wall regions are unimportant (therefore, this is a much better mode for short cylinders than TM_{010}), but the sheath close to the cylindrical walls is relatively important in this mode. An interesting feature of the TE_{011} mode is its de-emphasis of both the regions near the cylindrical and flat end walls, and it may therefore appear to be the most desirable probing field. In this mode, however, the important central region is completely ignored, indicating its lack of usefulness in the case of centered plasma containers whose radial dimension is a small fraction of the cavity radius.

The rectangular TE_{101} mode de-emphasizes four of the six wall regions. For reasons of mode purity, the height in the field direction (x direction) should be the smallest dimension. This means, unfortunately, that the sheath areas nearest the two largest walls are emphasized most by this field.

The differences in these weighting functions produce significant differences in the correction factors associated with each of these modes. Earlier studies[7] considered the cylindrical TM_{010} probing mode only, since this is the onle useful mode for one-dimensional geometries. As a consequence, correction factors evaluated for this mode have been used in the past to correct experimental data

obtained with other probing modes, a procedure which can introduce significant errors.

e) Filling factors. Some or all of the dimensions of the plasma container may be smaller than the cavity dimensions. We take account of this effect through a group of dimensionless parameters, γ , the ratio of the appropriate container and cavity dimensions, e.g. $\gamma_r = r_o/r_1$, $\gamma_z = z_o/z_1$, etc., where r_o and z_o indicate the plasma container dimensions. The subscript on γ indicates which one of the coordinates is considered. For cylindrical geometry, we usually give data for four γ values: $\gamma = 1$ (complete filling, which means $\gamma_r = \gamma_z = 1$), $\gamma_r = 1/2$ (which implies here $\gamma_z = 1$), $\gamma_z = 1/2$ (which implies $\gamma_r = 1$) and $\gamma = 0$ (i.e. $\gamma_r = \gamma_z = 0$ or a uniform probing field). In the case of the TM_{010} mode, the set with $\gamma_z = 1/2$ is omitted because of its triviality; in the z direction, the probing field is constant and the conditions are really the same for any value of γ_z in that case.

f) Fundamantal Diffusion Lengths

As noted in the earlier sections, one of the parameters which is required in evaluating the various normalized quantities, such as β , is the fundamental mode diffusion length, Λ . For simple geometries, Λ is readily obtained by separation and solution of the diffusion equation, $\partial n/\partial t = D_a \nabla^2 n$, subject to the condition that n goes to zero on the boundaries of the plasma container. Thus, for a plasma container in the form of a right circular cylinder (dimensions r_o, z_o) one has $1/\Lambda^2 = (2.4/r_o)^2 + (\pi/z_o)^2$, for a rectangular parallelepiped (dimensions x_o, y_o, z_o), $1/\Lambda^2 = \pi^2 (1/x_o^2 + 1/y_o^2 + 1/z_o^2)$, and for a sphere (radius r_o), $\Lambda = r_o/\pi$. For more complicated plasma container geometries, e.g. a cylinder with conically tapered ends[10], it is

necessary to evaluate Λ by computer solution of eq. (6) or eq. (13) with the recombination term set equal to zero. In this case, the final time constant, T_f, of the decay in the late afterglow is related to Λ by $\Lambda = (D_a T_f)^{1/2}$.

III. Results

a) One-dimensional geometries. The results for simple, one-dimensional container shapes are given in the fig. 2 through 7. From fig. 1, one finds that the three different geometries as presented here have increasing surface-to-volume ratio; thus a comparison of the results displays the effect of the g-values. Since the weight functions E^2 in eq. (9) affect the results strongly, we have compared the results for the case of a constant probing field, $\gamma = o$, only.

Furthermore, such a comparison can be made for k=0 only, because only then are the mean initial densities the same for parallel plates, infinite cylinders and spheres. For $k \neq o$, the initial mean densities are different; for example, for k=2 their ratios can be shown to be approximately 1:2:4. If k is, in each case, adjusted to provide the same initial average, the results may again be compared. However we then arrive at nearly the same conclusions as for the k=0 cases, which we now compare.

As can be seen from fig. 2, 3b and 4 at constant β, the linear ranges f decrease and the corrections Δ increase as the surface-to-volume ratio g increases. We thus see that a relatively large surface increases the effect of diffusion loss markedly. When we compare the parallel plate case with the sphere, we note that approximately equal f-values and Δ-values are found in fig. 2 at twice the β-values of fig. 4. We thus conclude that a 50% increas in the surface-to-volume ratio may be offset by a 50% reduction of the diffu-

sion coefficient D_a (which enters reciprocally in the expression for β), leading to essentially unchanged f and Δ -values.

This conclusion is further confirmed, to some degree, by comparison of other geometries with different g-values. The f and Δ -curves for the infinite cylinder (Fig. 3b), whose g-value is 30% larger than that of the parallel plate configuration, nearly agree with those given in fig. 2 as β is increased by 30%, and similar observations can be made for some finite cylinders with the same and higher g-values, fig. 13. In comparing other geometries, however, both the f-curves and Δ -curves exhibit different curvatures (for example compare the case of a cube, fig. 20, with the parallal planes) and the simple relation noted above can not be pushed too hard. Thus, qualitatively, an increased g-value leads to a stronger influence of diffusion and is comparable to an increased diffusion coefficient in geometries having smaller g-values (provided comparisons are made with comparable probing field distributions and initial density distributions).

By comparison of fig. 3a and 3b it can be seen that the effect of a probing field on the f and the Δ versus β curves is much stronger than the effect of g. The much larger f's and smaller Δ 's in fig. 3a are due to the de-emphasis of some wall areas by the weight function E^2 (eq. 3), especially for the case of equal container and cavity dimensions ($\gamma = 1$).

Since in most experiments, the value of β is not known beforehand (because of the unknown α and n_o values) we give our corrections Δ as function of the linear range f, a directly measureable quantity, see figs. 5 through 7. In this representation, for k=o and γ=o, the curves of Δ versus f agree closely for the three container shapes under consideration. In this presentation, the effect of the different g-values is thus automatically eliminated.

Our results for the sphere and for the infinite cylinder, for k=o and k=1, are found to be in rather good agreement with the results of Gray and Kerr[7], though certain small deviations occur. We verified their computations of the $1/\bar{N}$ versus τ curves*, as far as they are given in their paper [7], yet we found slightly different f and Δ values, in some cases. Thus we conclude that these authors have used a somewhat different evaluation procedure. These observed deviations are very little, though, and we feel that our work essentially confirms the earlier results.

b) Finite cylinders. The computed values of $N(r,z,\tau)$ which illustrate the evolution of the spatial distributions for a finite cylinder ($r_o=z_o=3.96\,\Lambda$), are given in fig. 8 for $\beta=550$. Three different initial distributions are assumed. The uniform initial density distribution (k=0) changes rapidly in appearance; in particular the sharp edges smooth out rapidly in the wall areas, and after a short time, $\tau\sim$ a few hundredths, a nearly time-independent "stable"form of distribution has been established. There is very little change in this distribution until τ approaches the values of 0.2 to 0.3. For larger times, above 0.4 or 0.6, the distribution approaches a fundamental diffusion mode distribution, which is maintained after the time $\tau=2$.

---

* There is only one exception, their fig. 8, which we believe is wrong in the time interval $o\leq\tau\leq o.o5$. Our computation gives an approximately linear rise of the same slope as for $\tau=o.o5$, but not the steep slopes they obtained, presumably by using too large time increments in this case.

The evolution of an initial fundamental mode diffusion distribution is shown in fig. 8. Again we find (at the same β - value) a very rapid formation of the "stationary" distribution and slow return to the diffusion distribution. For comparison, the case k=2 has also been illustrated. It can be seen that here the initial extent of the plasma is somewhat restricted, approximately to one-half the container dimensions, if the surface where the densities are half the central densities is taken as the boundary of the plasma. However, the differences in the distributions, for different initial distribution, are small for times above $\tau \cong 0.1$.

It is of interest to note that for this β value (550), under favorable conditions (such as $\gamma_z = \gamma_r = 1$), the linear portion of the $1/\bar{N}$ versus τ curves lasts from $\tau = 0$ to $\tau = 0.2$ and under less favorable conditions ($\gamma \approx 0$) only from 0 to 0.025. In the latter case, the differences in $N(r, z, \tau)$ due to different k's are quite significant.

In order to present the data for finite cylinders, a new parameter z_o/r_o, the ratio of container length to radius, is introduced. For most practical cases, this ratio will be of the order of unity, i.e. between 0.1 and 10. According to eq. 17 or fig. 1, this means that the surface-to-volume ratio g will practically always be close to 1. Thus the small changes of the parameter g may be disregarded, if different finite cylinders of practical interest are to be compared.

The importance of the new parameter z_o/r_o at large filling factors ($\gamma \approx 1$) is obvious. If we compare the results of fig. 9a with fig. 10a, we find very different f and Δ-values, the only difference being the parameter z_o/r_o, which equals 1 in fig. 9 and 2.3 in fig. 10. These differences nearly disappear, though, as γ approaches 0. It thus is clear that the probing field,

which emphasizes certain wall areas, depending upon z_o/r_o, is responsible for these differences. Similarly we note by comparison of fig. 9a, b and c (or fig. 10a, b and c) that for a constant z_o/r_o, but varying probing fields, very different f and ν-values result, for the same reason.

The significance of the parameter z_o/r_o for the experiment can be seen from the figs. 11 through 19, where the corrections Δ as function of f are plotted for several microwave field modes and filling factors. Particularly for k=0 and small f values ($\lesssim$ 10), but to a lesser extent also for k=2 and k=1, an influence of z_o/r_o is found. For γ =0 (fig. 13) very small differences (if any) can be seen, indicating the relative unimportance of small changes in g for these cylinders.

A comparison of the results for finite and infinite cylinders with a TM_{010} probing field (see Table I), figs. 6a, 11, and 12, shows that the corrections Δ are larger for the finite cylinder. (The differences are more pronounced if the f's and Δ's at an equal β are compared.) This is easily understood from the importance of the flat end wall areas, for this mode, whereas the density gradient in the z-direction is absent in the infinite cylinder case. This is one reason why the infinite-cylinder correction factors [7] lead to <u>under</u>-correction of recombination data obtained with finite cylinders when scaling to the same Λ or β values is used.

Table 1. Cylindrical container dimensions used in the computations.

z_o/Λ	r_o/Λ	z_o/r_o	g
∞	2.4	∞	0.831
13.6	2.475	5.5	0.954
6.28	2.775	2.3	1.04
4.45	3.41	1.3	1.04
3.96	3.96	1.0	1.01
3.56	5.09	0.7	0.954
3.26	9.3	0.35	0.831

c) Parallelepipeds. For rectangular parallelepipeds, two new parameters, x_o/z_o and y_o/z_o, are used. Again, it is assumed that these parameters are, for most practical purposes, roughly of the order of unity, which means g-values of about 1. Under this assumption, g can again be considered to be nearly constant, and we may disregard g when different parallelepipeds are to be compared.

In fig. 20 the f and Δ versus β curves for a cube are given. (In practice, cubes are unlikely to be used because of the desired mode purity. Ordinarily, one side will be made somewhat smaller. However, because of the little influence of g and the constancy of the field in the x direction, the cube data are in fact a very close approximation to many real cases). These values represent, for a constant probing field ($\gamma = 0$), the smallest f's and Δ's of this paper, because of the large g value (1.1). Figs. 21 and 22 present a survey of all our computations for this case (see Table 2) and show that the parameters x_o, y_o, z_o are of modest influence for moderate variation in their values.

Table 2. The parallelipiped dimensions used in the present computations. (Lower case letters refer to Figs. 21 and 22).

	x_o Å	y_o Å	z_o Å	g
a	5.44	5.44	5.44	1.10
b	4.21	5.27	10.5	0.95
c	3.49	9.95	10.47	0.95
	3.4	8.7	26.2	0.83

IV. Conclusion

A numerical solution has been obtained to eq. 6, which describes the electron density decay in an afterglow, in the absence of electron production processes and under the assumption that ambipolar diffusion and two-body volume recombination are the only electron removal processes. We have considered several one-dimensional geometries, "two"-dimensional finite cylinders and three-dimensional, rectangular parallelepipeds. From these solutions, we have calculated the time-dependence of the mean electron density for several modes of the microwave probing field, which have then been used to derive corrections to be applied to the measured slopes of the experimental $1/\bar{n}$ versus t curves in order to obtain the actual two-body recombination coefficient α . It is shown that these corrections depend upon the number of dimensions in the Laplace operator, the surface-to-volume ratio g of the container, the microwave probing field mode and certain dimensional parameters such as z_o/r_o (for finite cylinders). It has been found that, for many practical purposes, a number of parameters can be disregarded.

The results of an earlier one-dimensional study[7] have been confirmed and extended. The need for a more-dimensional treatment for most cases of practical interest has been demonstrated. In addition, a third initial distribution ("constricted" or squared diffusion distribution) besides the two previously considered [7,8] (namely, recombination and diffusion controlled distributions) has been included. The "constricted" distribution has been

found to be of practical interest in recent studies[10, 11], especially at higher pressures where the initial density distribution is approximately described by a function of the form of eq. (21) or (22), with an exponent between 1 and 2, rather than between 0 and 1 as has usually been assumed.

Finally, since in evaluating an experimental measurement the value of α (and therefore of β) is initially not known, one uses the value of the linear range f, determined from the $1/\overline{n}$ versus t curve, to obtain a preliminary value of α from the measured slope, a, by use of the Δ versus f correction curves and eq. (12). With this value of α, one computes β and then obtains a more accurate correction factor from the Δ versus β curve. If the value of α so determined differs appreciably from the preliminary value, a new value of β is computed and a new correction factor, Δ, is determined. This iterative procedure avoids the possibility of error that an enhanced or diminished f value [e.g., resulting from ionization or electron loss processes not considered in the solution of eqs. (6) or (13)] would introduce.

Acknowledgement

The authors wish to thank Mr. K. H. Wiemer for his help during the computations. The generous support of the U. T. Computer Center, of the Air Force Research Office, and of the Joint Services (Electronics Program) is also gratefully acknowledged.

Appendix. The geometry factor G introduced above can be expressed in terms of elementary functions, in many cases. For cylindrical containers and cylindrical cavities, we obtain for a T M_{010} mode ($x=2.4\,r_o/r_1$)

$$G = (r_1 / r_o)^2 \cdot \frac{J_1^{\,2}(2.4)}{J_o^{\,2}(x) + J_1^{\,2}(x)} \cdot (z_1 / z_0) \qquad (28)$$

and for a TE_{011} mode ($x = 3.83\ r_o/r_1$)

$$G = (r_1/r_o)^2 \cdot \frac{J_o(3.83)\, J_1(3.83)}{J_1^{\,2}(x) + J_o(x) J_1(x)} \cdot (z_1/z_o) \cdot \left(1 - \tfrac{1}{2} \cos\left(2\pi \frac{z_1}{z_o}\right)\right) \qquad (29)$$

The $J_n(x)$ are ordinary Bessel functions, and $J_n^{\,2}(x)$ means the square of $J_n(x)$.

~~Erratum~~

~~The squared field for a cylindrical TE_{111} mode (page 15) should read ($x=1.84\,r/r_1$):~~

$$~~E^2 = \left\{ \frac{1}{x^2} J_1^{\,2}(x) + J_1'^{\,2}(x) \right\} \cos^2 \pi\, z/z_1~~$$

1. H. Margenau, Phys. Rev. 69, 508 (1946)
2. M.A. Biondi, Rev. Sci. Instr. 22, 500 (1951)
3. D.J. Rose and S.C. Brown, J.Appl. Phys. 23, 1028 (1952)
4. L. Goldstein and G. Geyger, Elec. Commun. 29, 243 (1952)
5. M.A. Biondi, "Afterglow experiments - Atomic collisions of electrons, ions, and excited atoms" in Methods of Experimental Physics, vol. 7, L. Bederson & W.L. Fite, editiors, Academic Press, N. York (1968), to be published.
6. J.C. Slater, Rev. Mod. Phys. 18, 441 (1946)
7. E.P. Gray and D.E. Kerr, Ann. Phys. (N.Y.) 17, 276 (1962)
8. H. Oskam, Philips Research Reports 13, 335 (1958)
9. W.H. Kasner and M.A. Biondi, Phys. Rev. 137, A317 (1965)
10. L. Frommhold, M.A. Biondi, F.J. Mehr, Phys. Rev., 165 (1968)
11. L. Frommhold, paper given at the 20th Gaseous Electronics Conference, 18-20 Oct. 1967, San Francisco. Abstract to be published in Bull. Am. Phys. Soc.
12. L. Collatz, " The Numerical Treatment of Differential Equations", Springer Berlin, 3rd edition (1960), p. 295.
13. R. Courant and D. Hilbert, Methoden der mathematischen Physik, vol. II, Springer Verlag, Berlin, 1937
14. Handbook of Mathematical Functions, edited by M. Abramowitz and I. A. Stegun, Nat. B. Standards, 1964, 3rd printing, p. 790.

Captions

Fig. 1: The normalized surface-to-volume ratio g for several simple container shapes, as function of their reciprocal length z_o, multiplied by π and the fundamental diffusion length Λ .

fig. 2: Δ and f values for a parallel plate geometry, for a uniform probing field ($\gamma = o$), as function of β . K is the exponent in the initial distribution, see sec. IIb. The circles, squares and triangles indicate the computed values used for plotting the curves.

fig. 3: Δ and f values for infinite cylinder geometry, as function of β . a) The probing field mode is TM_{o10} and the ratio of container to cavity radius, $\gamma_r = r_o/r_1$, equals 1 and 1/2, respectively. K is the exponent in the initial distribution. b) The probing field is assumed to be constant ($\gamma = o$) . The circles, squares and triangles indicate the computed values used for plotting the curves.

fig. 4: Δ and f values for spheres, as function of β . A constant probing field is assumed. K is the exponent in the initial distribution. The circles, squares and triangles indicate the computed values used to plot the curves.

fig. 5: Corrections Δ as function of f, for parallel plate "containers".

fig. 6: Corrections Δ as function of f, for infinite cylinder containers. a) $\gamma_r = 1$ and = 1/2. b) $\gamma = 0$.

fig. 7: Corrections Δ as function of f, for spherical containers. A constant probing field is assumed ($\gamma = o$).

fig. 8: Electron density distribution at different times in the afterglow, as function of r and z, for a finite cylinder. $r_o = z_o = 3.96\,\Lambda$, $\beta = 550$. The densities of this plot have to be multiplied by the time dependent factor N_o, which is given for each case. a) A constant initial distribution is assumed. b) A fundamental diffusion mode initial distribution is assumed. c) An initial "squared diffusion distribution", with an exponent K = 2, is assumed.

fig. 9: Δ and f values as function of β, for a finite cylinder with $z_o = r_o = 3.96\,\Lambda$, g = 1.01. $\gamma_r = 1$ and $= 1/2$.
a) TM_{010} mode, b) TE_{111} mode, c) TE_{011} mode probing field.

fig.10: Same as in fig. 9 a, b, c, but changed cylinder dimensions: $r_o = 2.775\,\Lambda$, $z_o = 6.283\,\Lambda$, g = 1.04.
a) TM_{010} mode, b) TE_{111} mode, c) TE_{011} mode.

fig.11: Corrections Δ versus f, for finite cylinders and a TM_{010} mode. The ratio z_o/r_o varies from .35 to 5.5, the filling factor being 1 ($\gamma_r = \gamma_z = 1$).

fig.12: Same conditions as in fig. 11, except $\gamma_r = r_o / r_1 = 1/2$.

fig. 13: Corrections Δ versus f, for finite cylinder geometry, and a constant probing field ($\gamma = o$). The ratio z_o / r_o varies from .35 to 5.5.

fig. 14: Corrections Δ versus f, for finite cylinders and a TE_{111} mode, $\gamma_r = \gamma_z = 1. z_o/r_o$ varies from .35 to 5.5

fig. 15: Corrections Δ versus f, for finite cylinders and a cylindrical TE_{111} mode, $\gamma_r = 1$ and $\gamma_z = 1/2$. z_o/r_o varies from .35 through 5.5

fig. 16: Corrections Δ versus f, for finite cylinders and a cylindrical TE_{111} mode, $\gamma_r = 1/2$ and $\gamma_z = 1$. z_o/r_o varies from .35 through 5.5

fig. 17: Same conditions as in fig. 14, except that a TE_{011} mode field was used.

fig. 18: Same conditionsas in fig. 15, except that a TE_{011} mode field was used.

fig. 19: Same conditions as in fig. 16, except that a TE_{011} mode field distribution was used.

fig. 20: Δ and f versus β for a rectangular parallelepiped with $x_o = y_o = z_o = 5.44 \Lambda$. Equal container and cavity dimensions have been assumed ($\gamma = 1$) as well as a constant probing field ($\gamma = o$). The field distribution corresponds to a rectangular TE_{101} mode.

fig. 21: Corrections Δ versus f for parallelepipeds and a TE_{101} probing field, for equal container and cavity dimensions. The meaning of the letters a,b,c can be seen from table 2. The two container dimensions listed under c) gave nearly the same data.

fig. 22: Same conditions as in fig. 21, except for a uniform probing field ($\gamma = 0$).

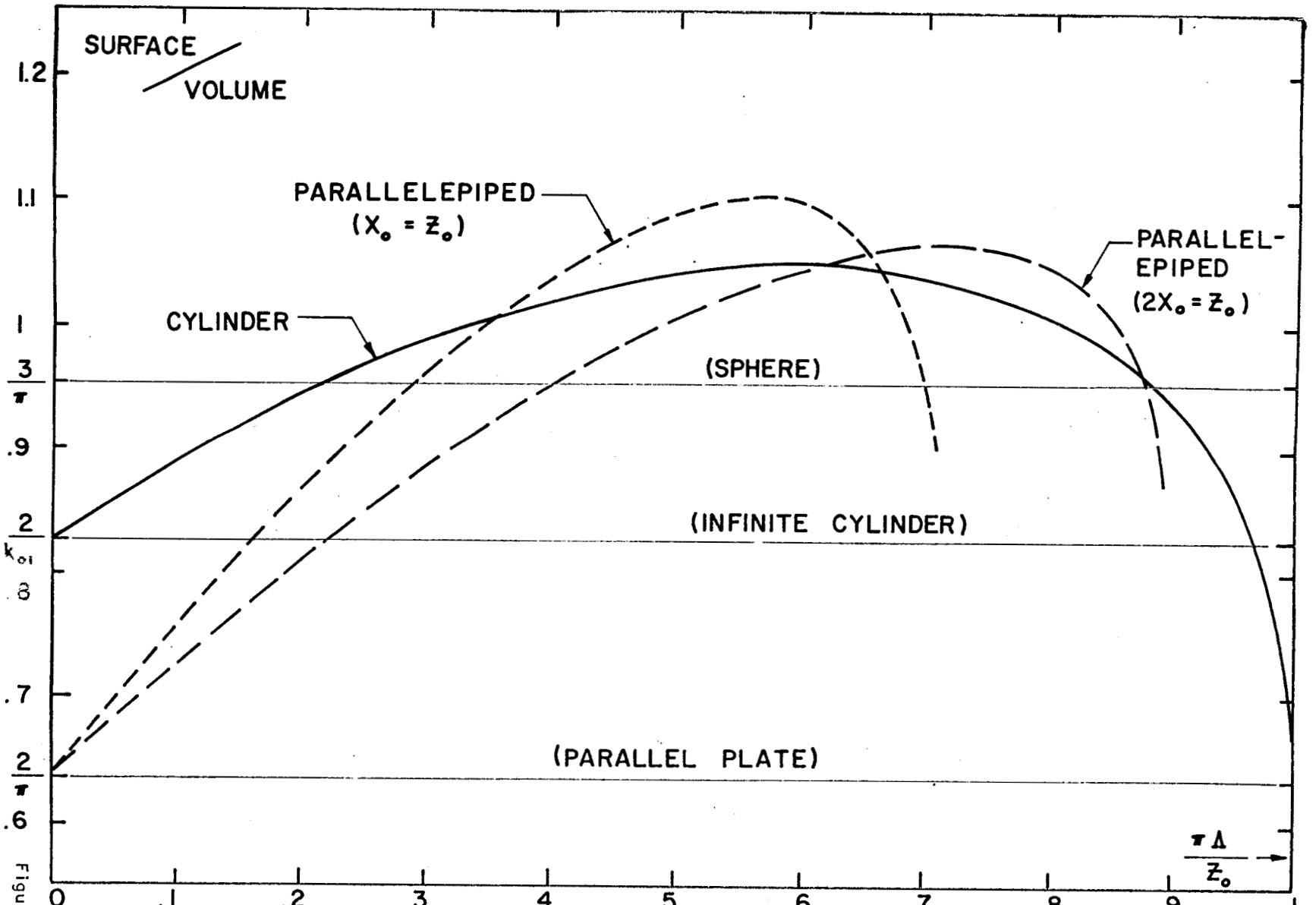
SURFACE
VOLUME
1.2
1.1
1
.9
.7
.6
PARALLELEPIPED
($X_o = Z_o$)
PARALLEL-
EPIPED
($2X_o = Z_o$)
CYLINDER
(SPHERE)
(INFINITE CYLINDER)
(PARALLEL PLATE)
k_δ
$\pi\Lambda$
Z_o
0
.1
.2
.3
.4
.5
.6
.7
.8
.9
1

Figure 1

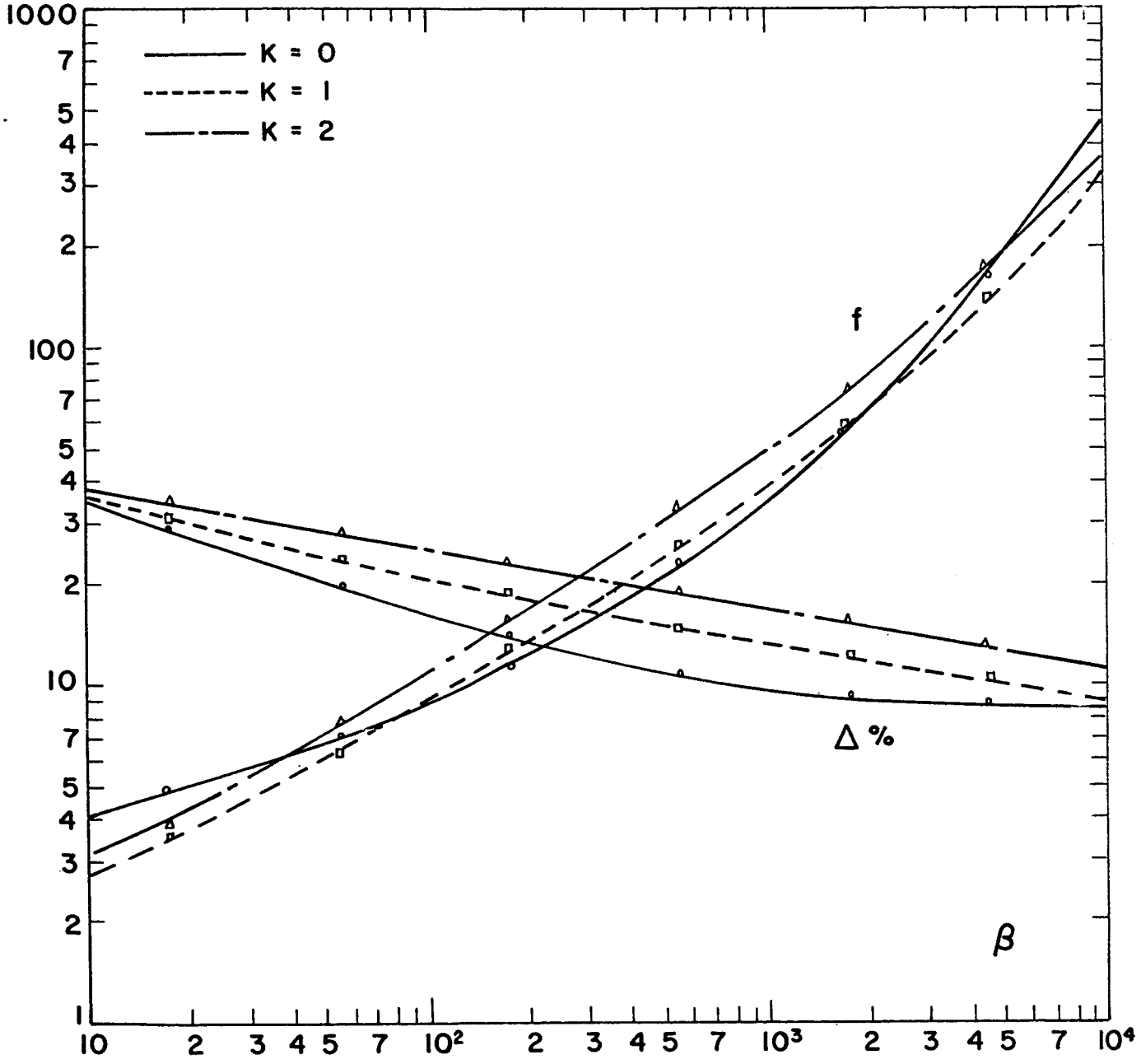
K = 0
K = 1
K = 2
f
Δ %
β
1000
7
5
4
3
2
100
7
5
4
3
2
10
7
5
4
3
2
1
10
2
3
4
5
7
10²
2
3
4
5
7
10³
2
3
4
5
7
10⁴

Figure 2

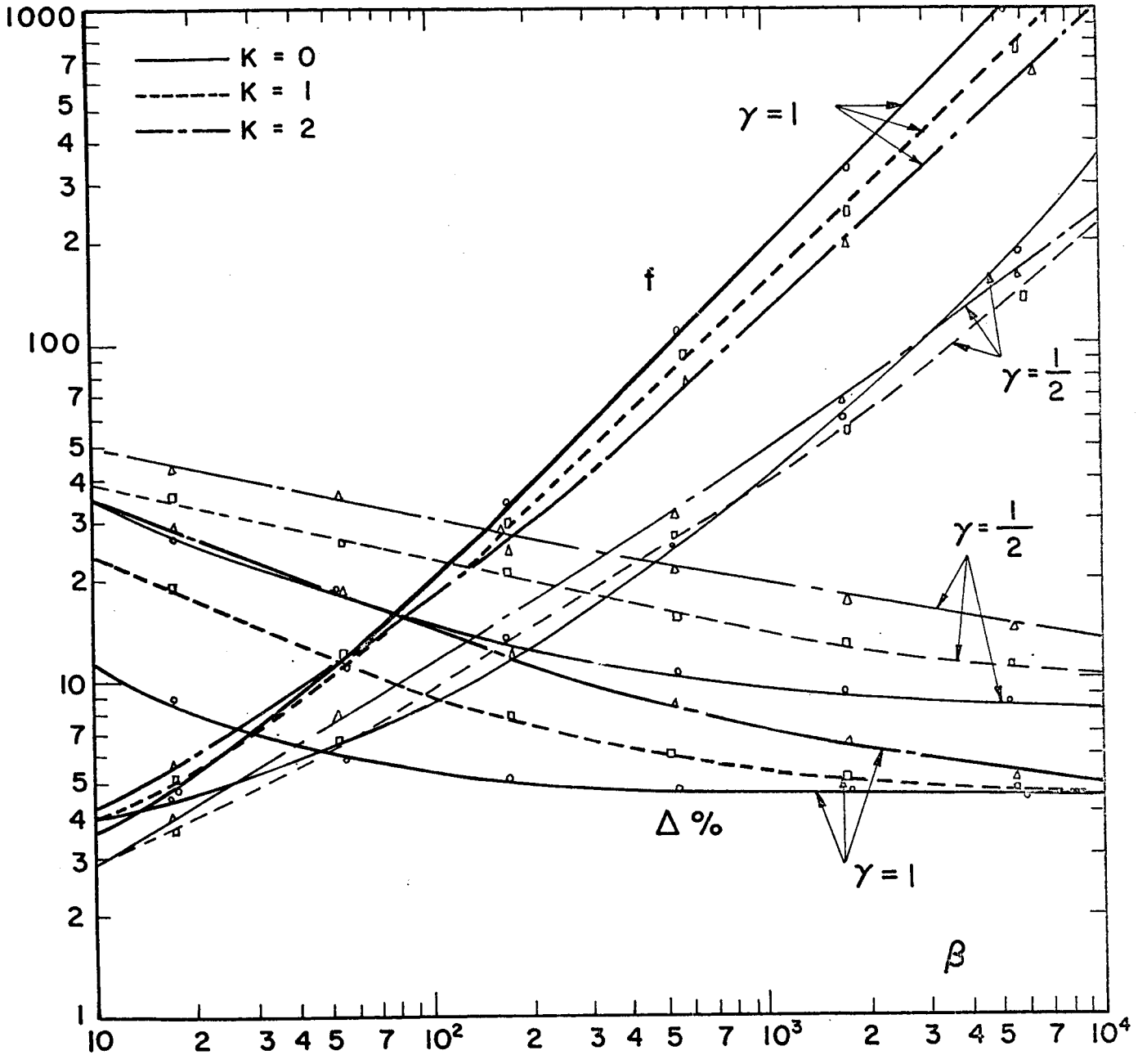
K = 0
K = 1
K = 2
γ = 1
f
γ = 1/2
γ = 1/2
Δ %
γ = 1
β
1000
7
5
4
3
2
100
7
5
4
3
2
10
7
5
4
3
2
1
10
2
3
4
5
7
10²
2
3
4
5
7
10³
2
3
4
5
7
10⁴

Figure 3a

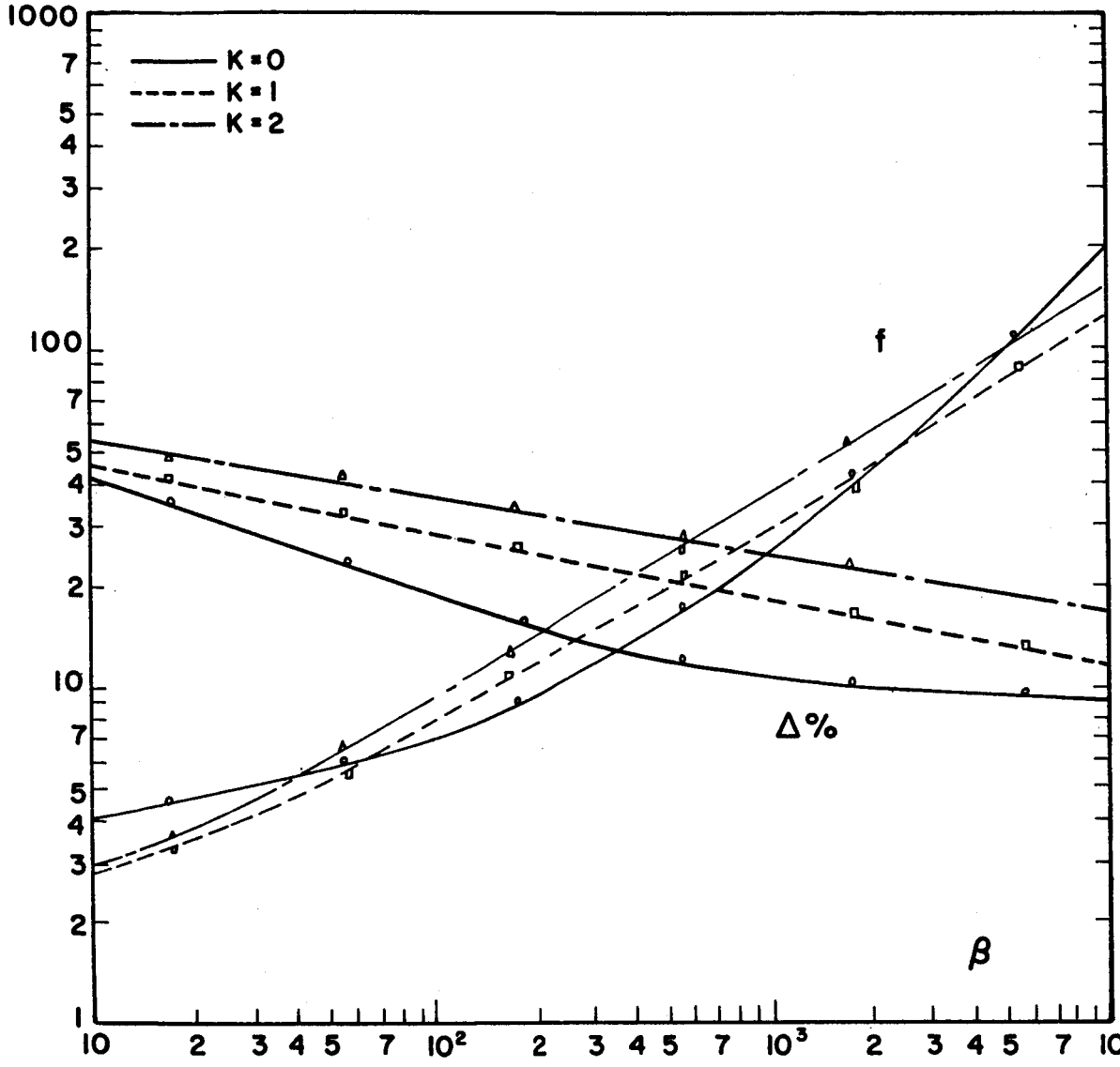
K=0
K=1
K=2
f
Δ%
β
1000
7
5
4
3
2
100
7
5
4
3
2
10
7
5
4
3
2
1
10
2
3
4
5
7
10²
2
3
4
5
7
10³
2
3
4
5
7
10⁴

Figure 3b

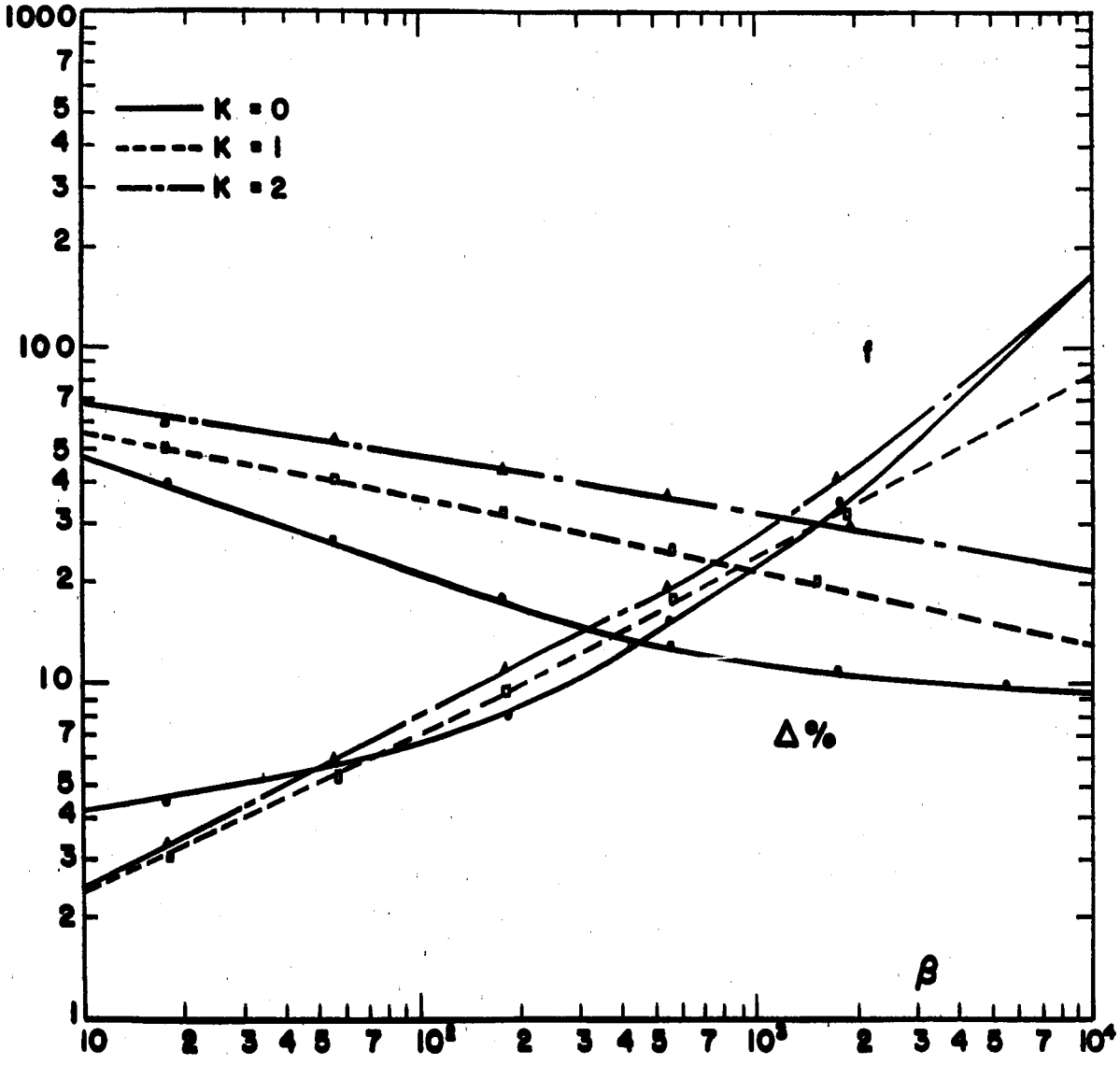
1000
7
5
4
3
2
100
7
5
4
3
2
10
7
5
4
3
2
1
K = 0
K = 1
K = 2
f
Δ%
β
10
2
3
4
5
7
10²
2
3
4
5
7
10³
2
3
4
5
7
10⁴

Figure 4

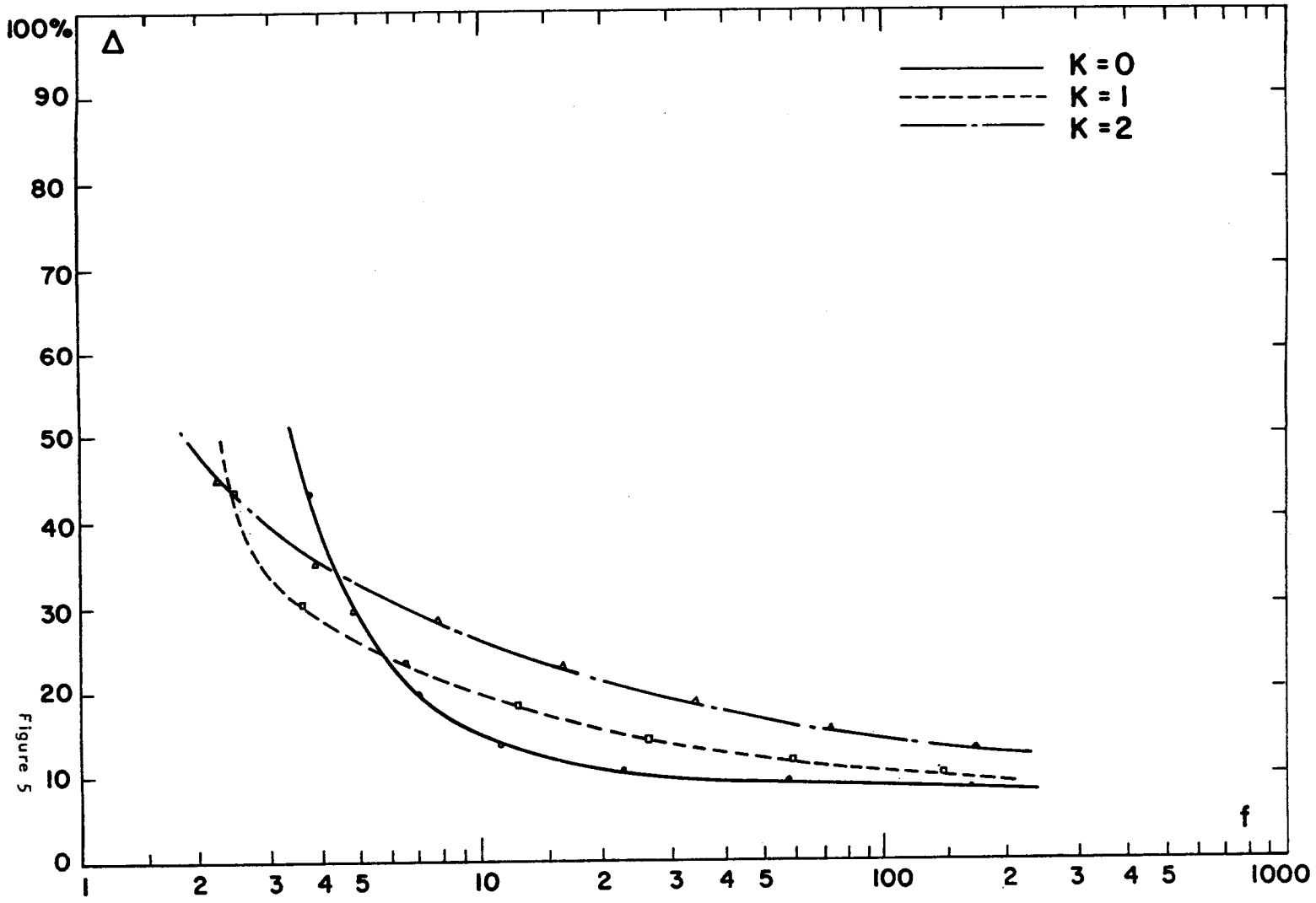
100%
90
80
70
60
50
40
30
20
10
0
Δ
K = 0
K = 1
K = 2
f
1
2
3
4
5
10
2
3
4
5
100
2
3
4
5
1000

Figure 5

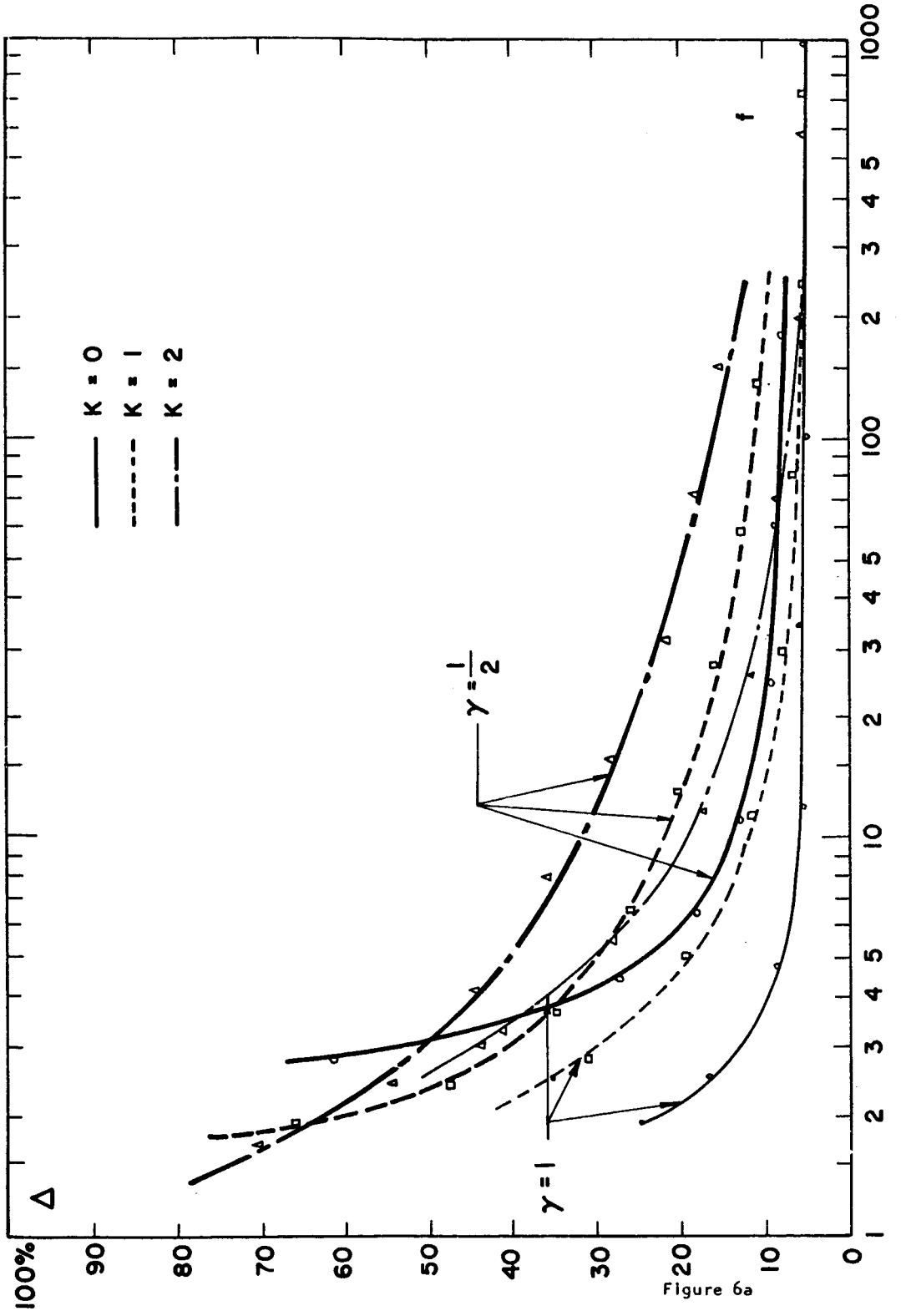

Figure 6a

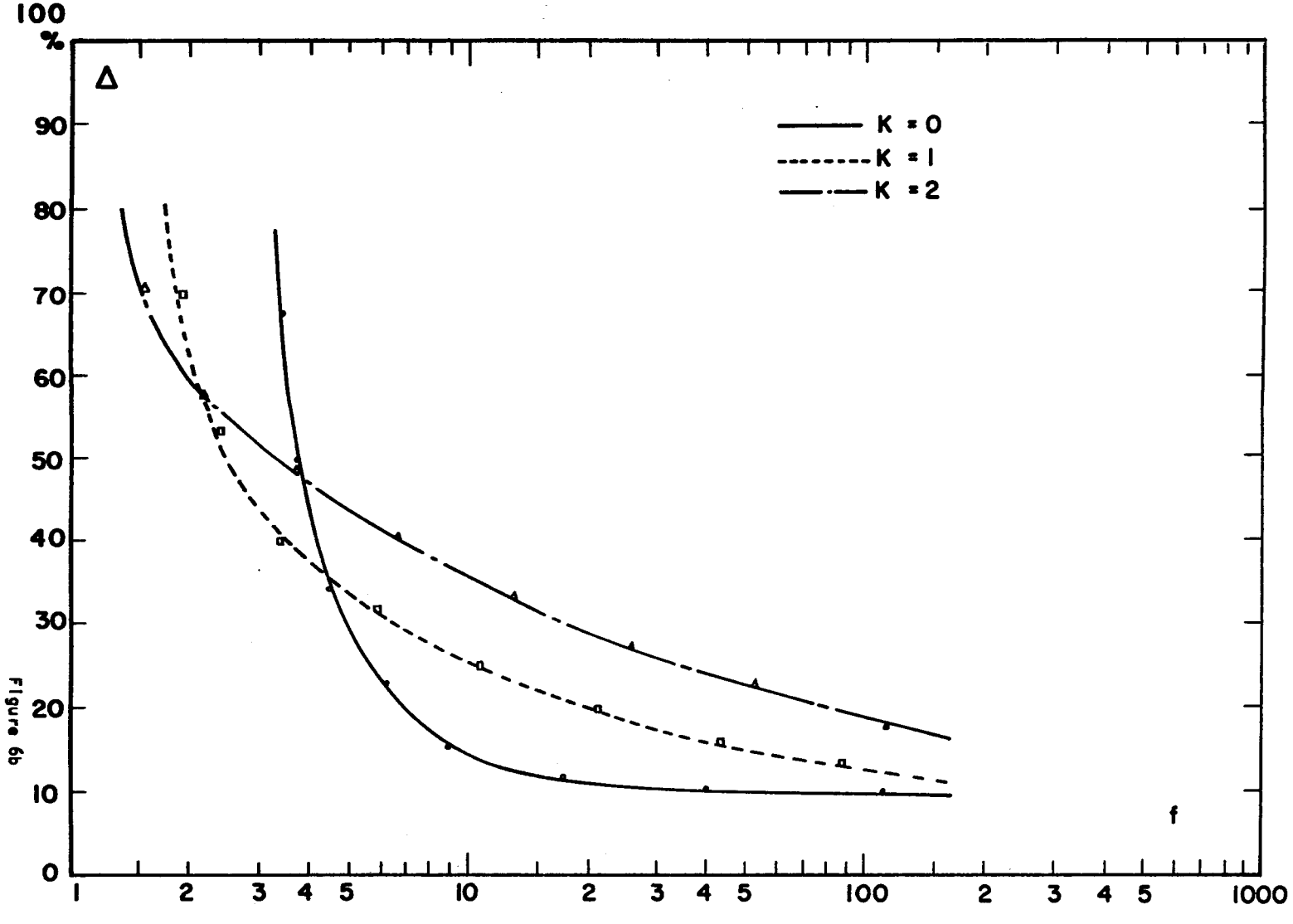
100
%
Δ
90
80
70
60
50
40
30
20
10
0
K = 0
K = 1
K = 2
f
1
2
3
4
5
10
2
3
4
5
100
2
3
4
5
1000

Figure 6b

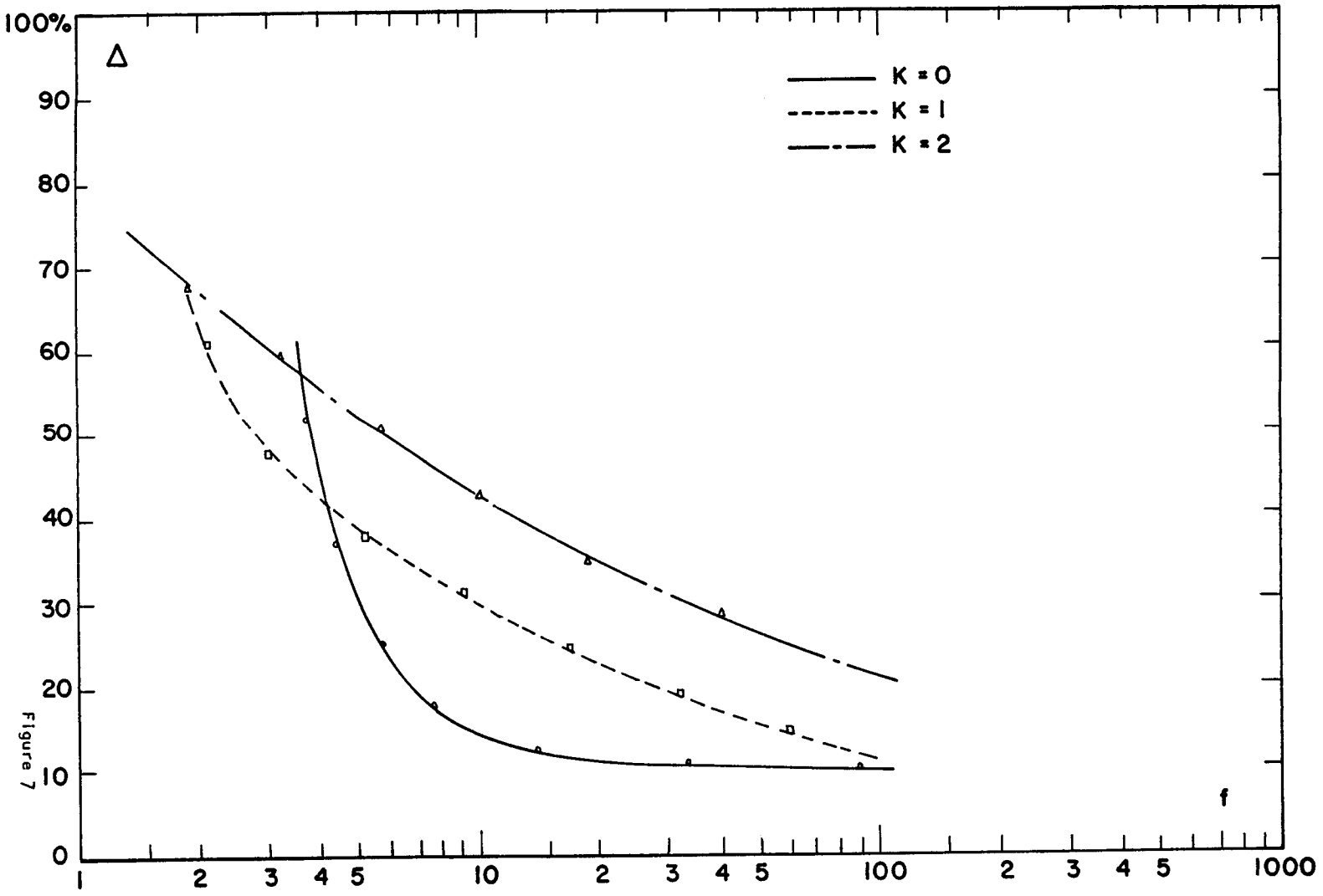
100%
90
80
70
60
50
40
30
20
10
0
Δ
K = 0
K = 1
K = 2
f
1
2
3
4
5
10
2
3
4
5
100
2
3
4
5
1000

Figure 7

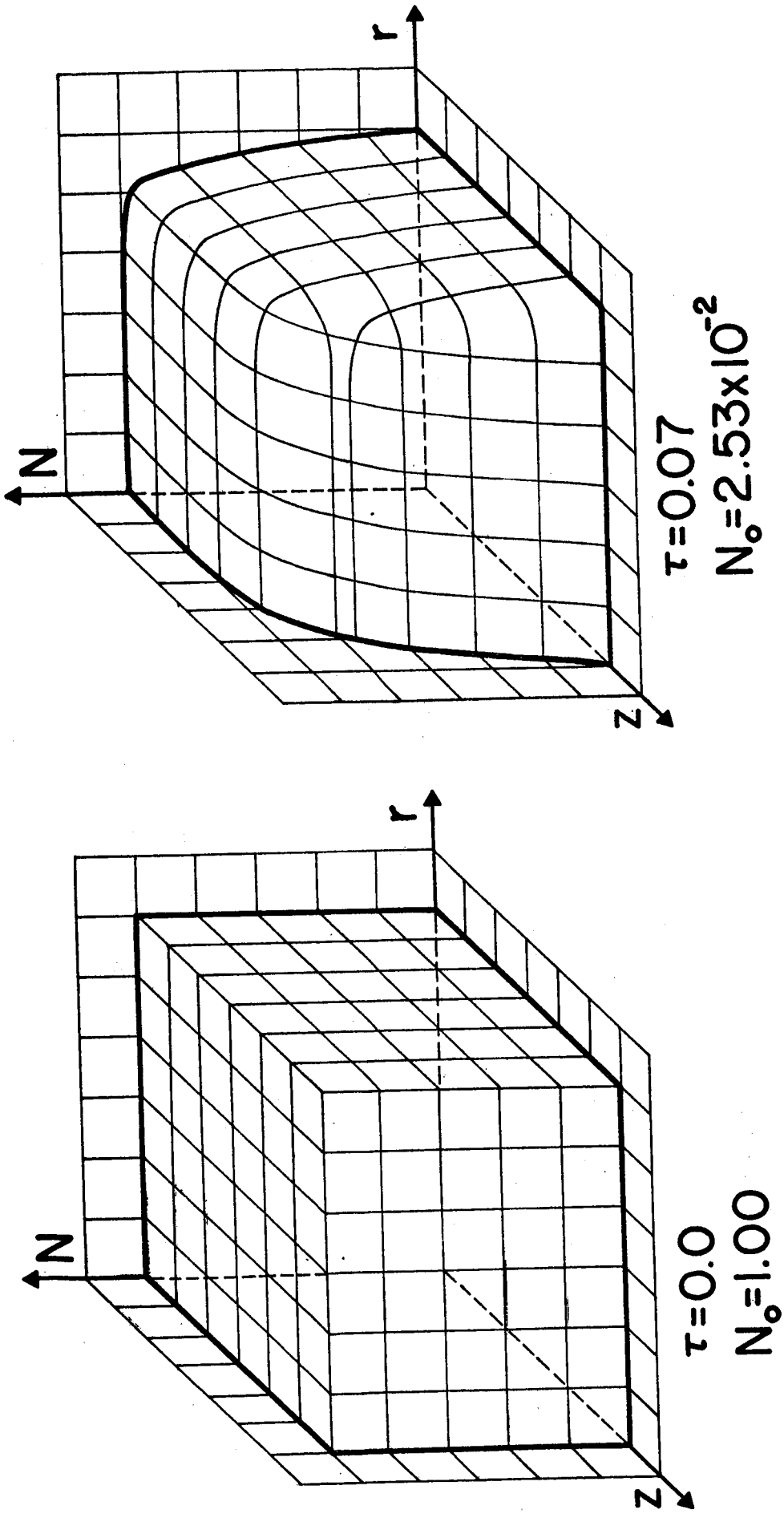

Figure 8A/1

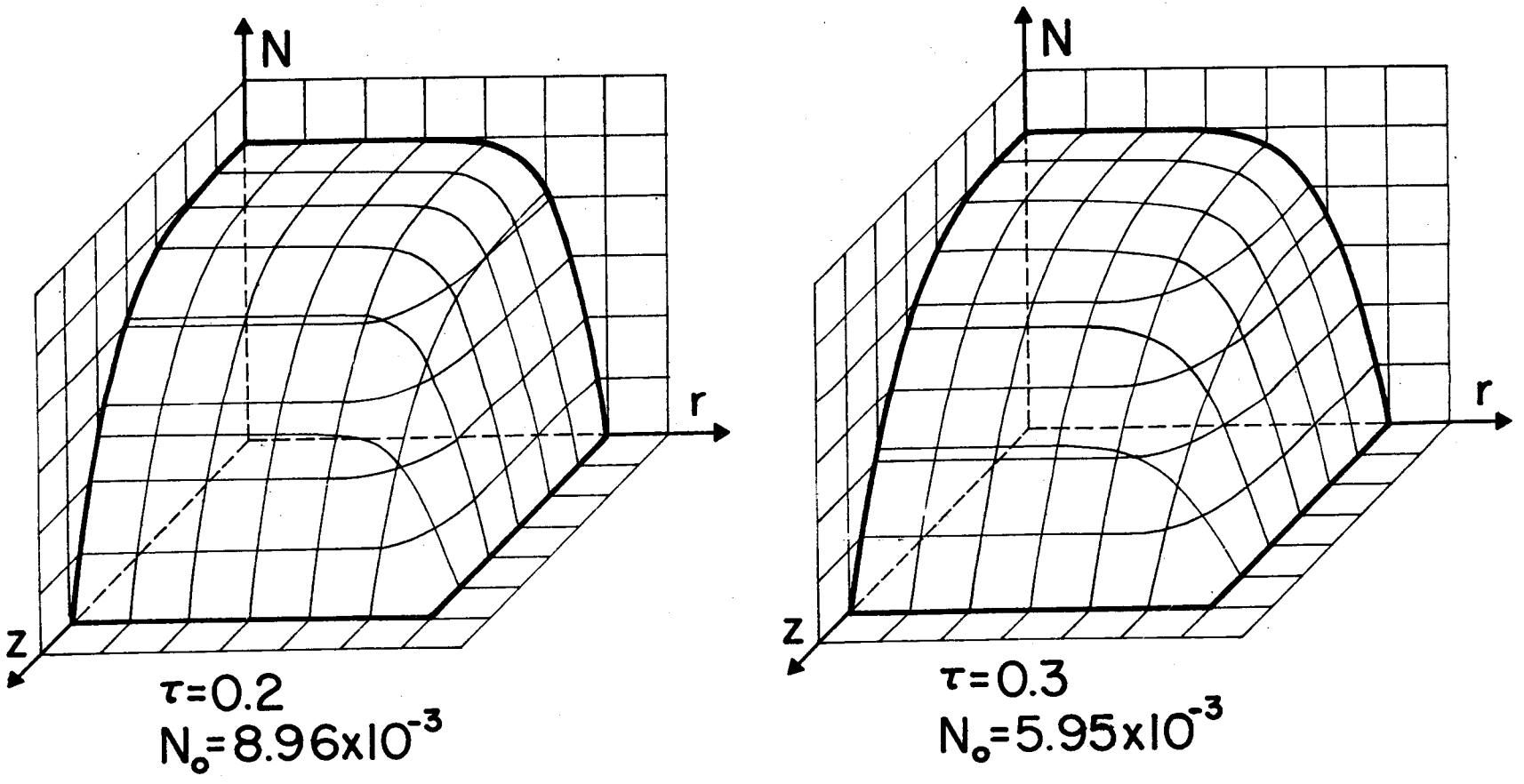

Figu

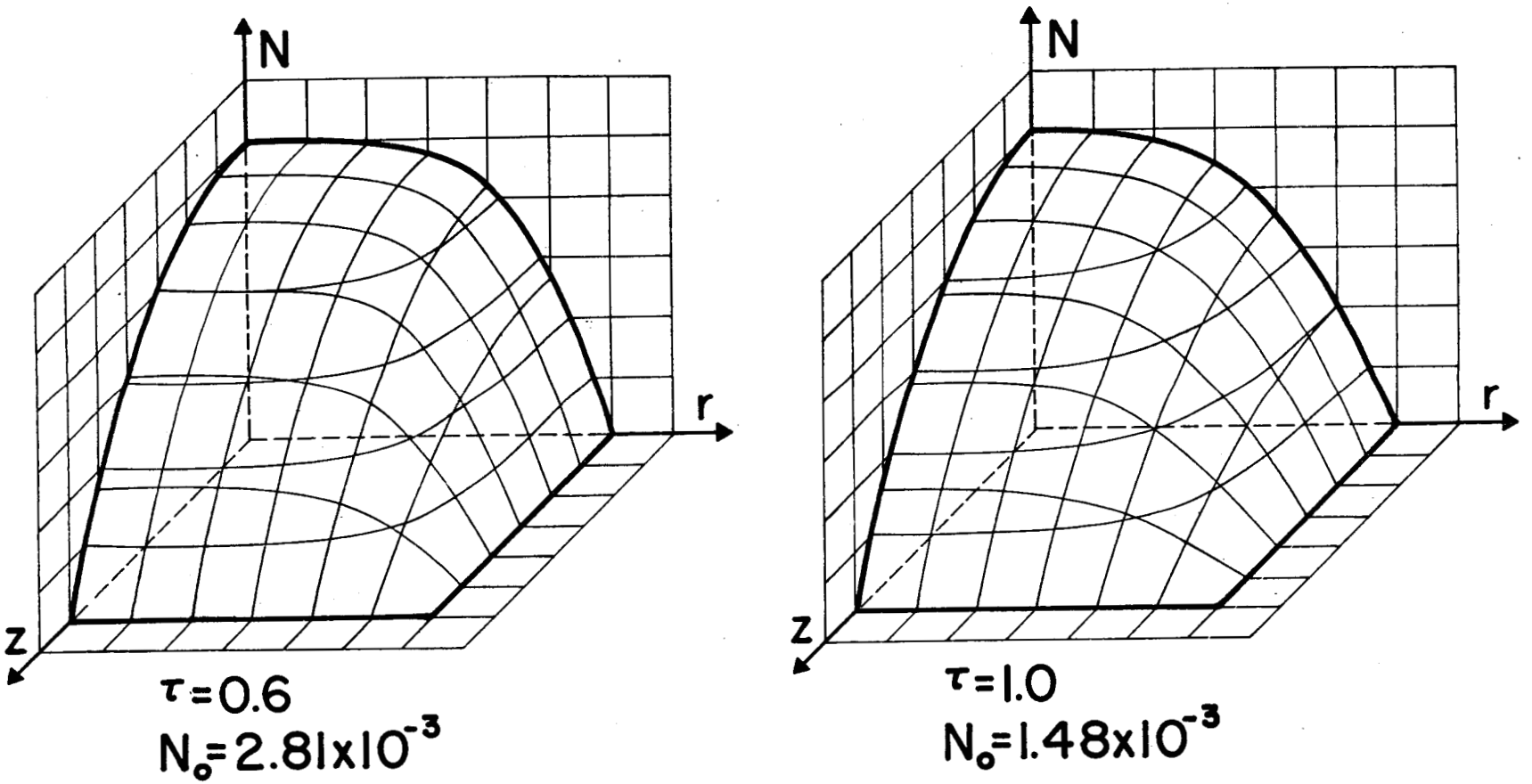

Figure 8A/3

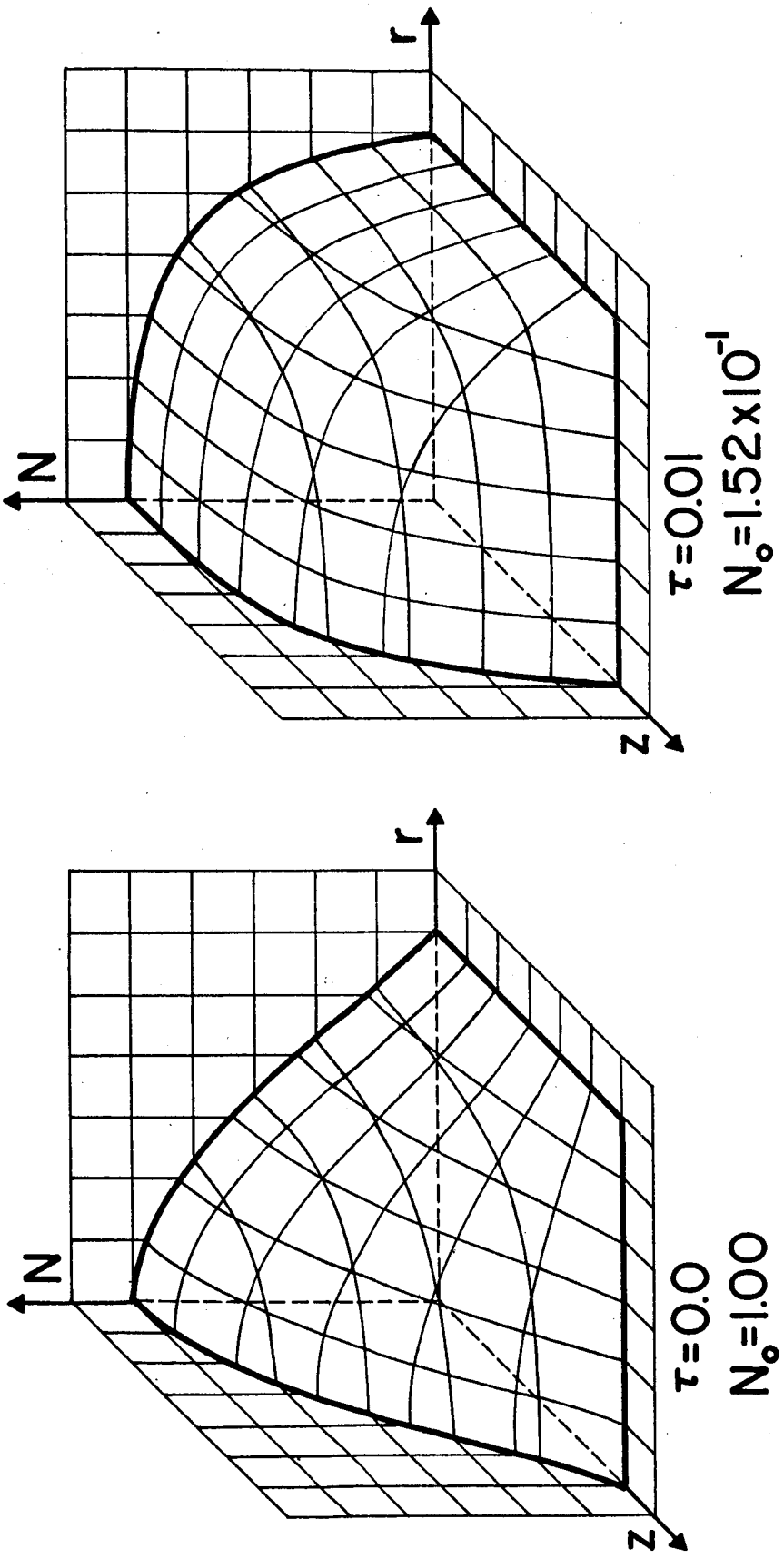

Figure 88/1

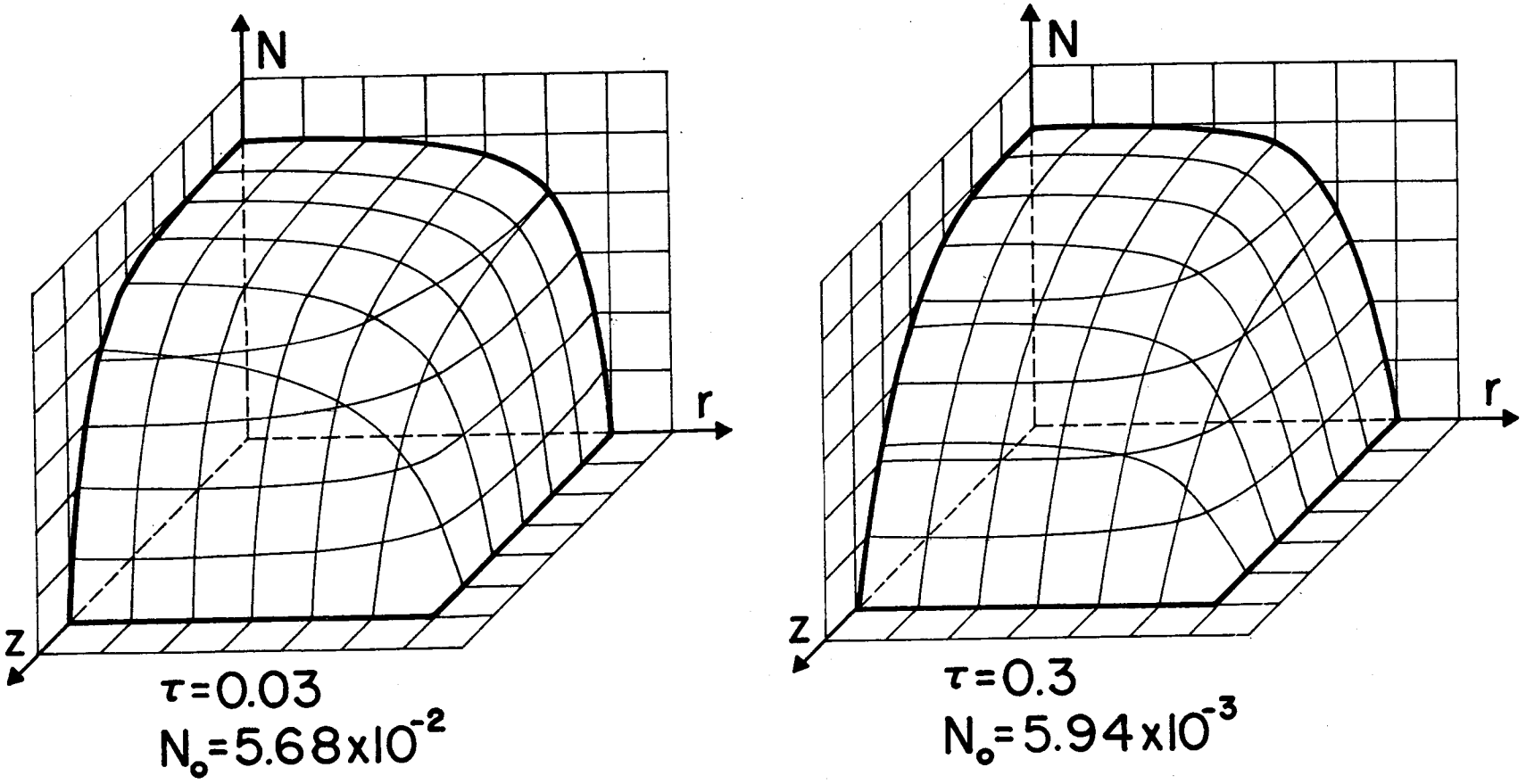

Figure 8B

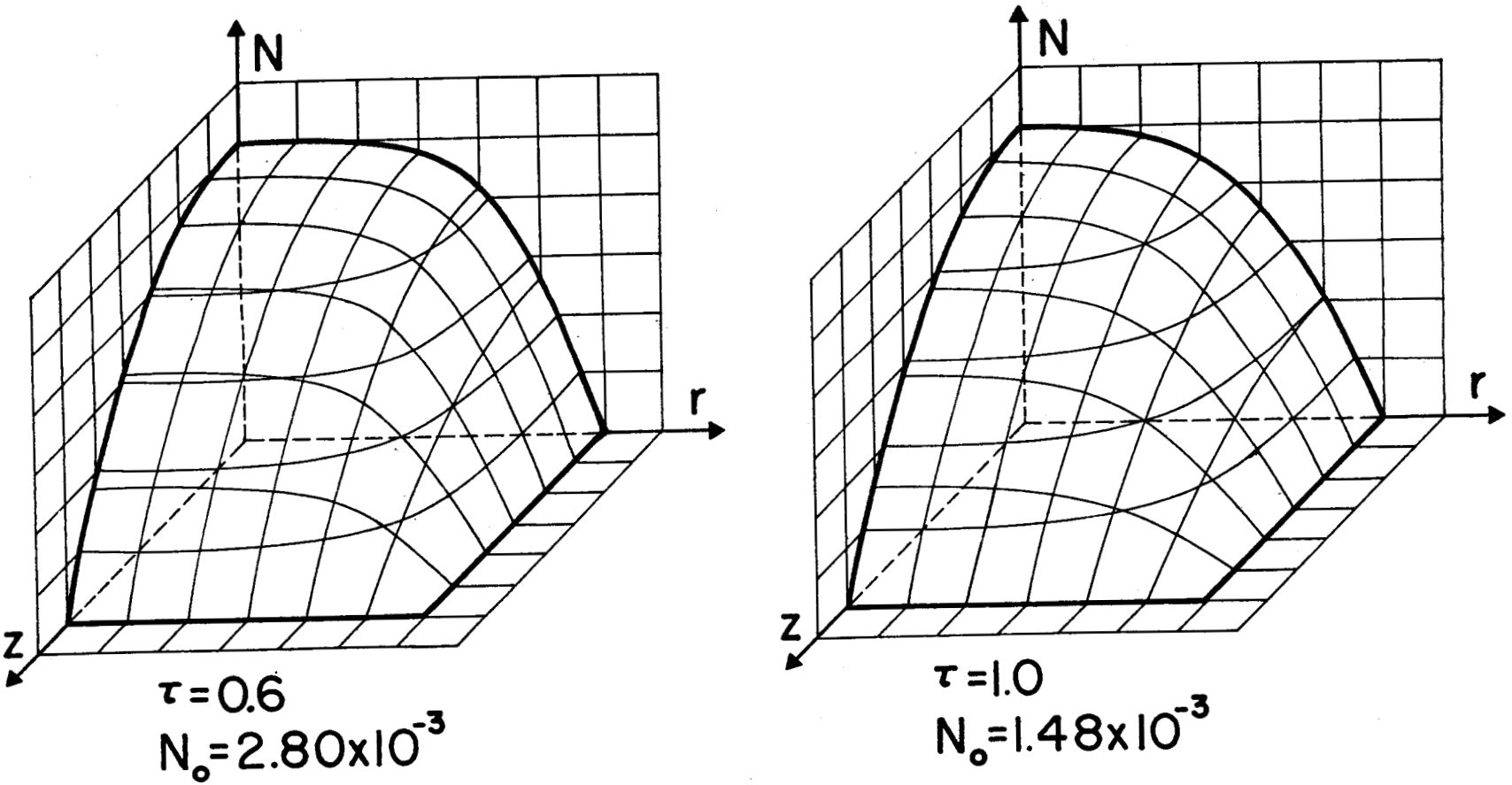

Figure 88/3

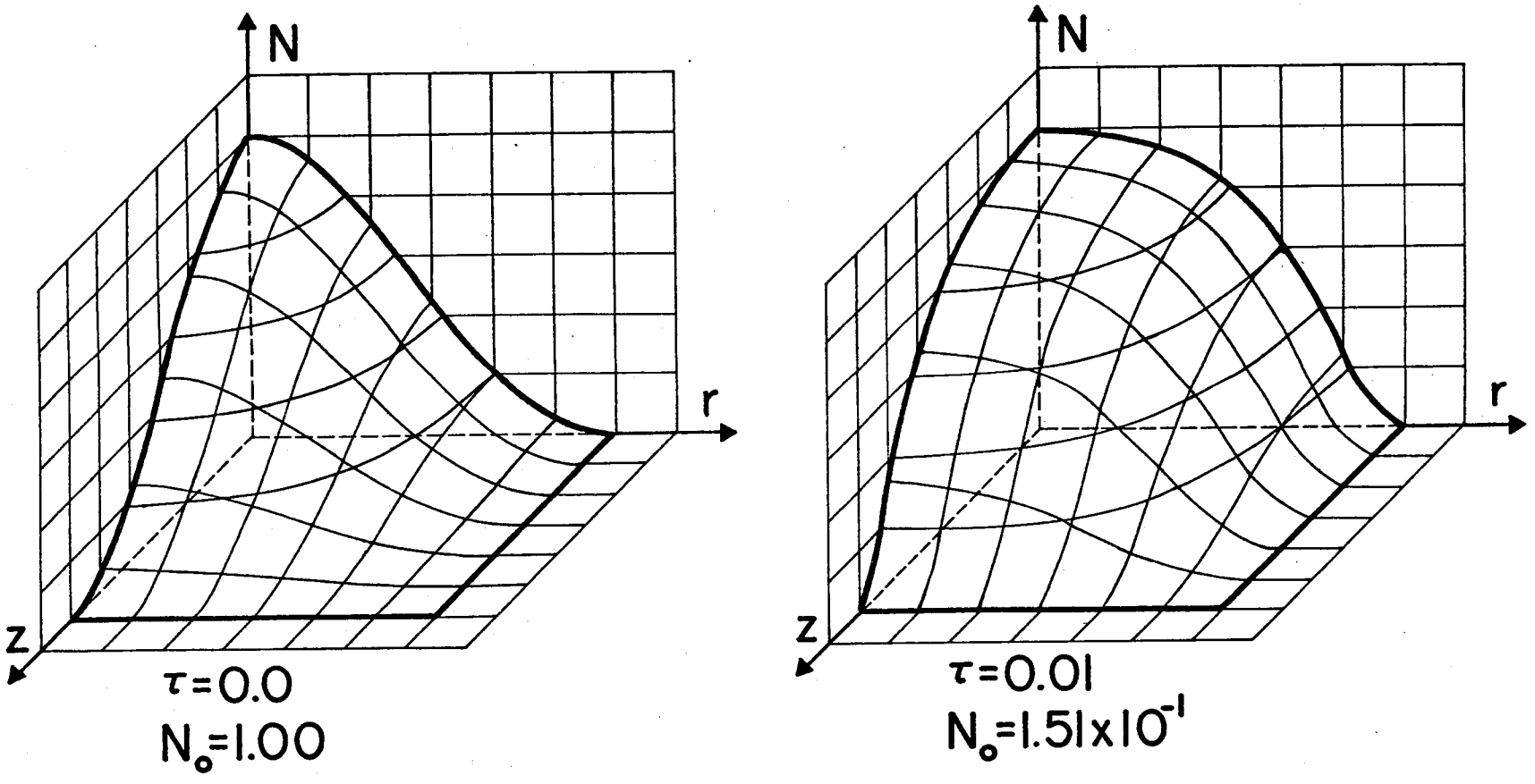

Figure 8C/1

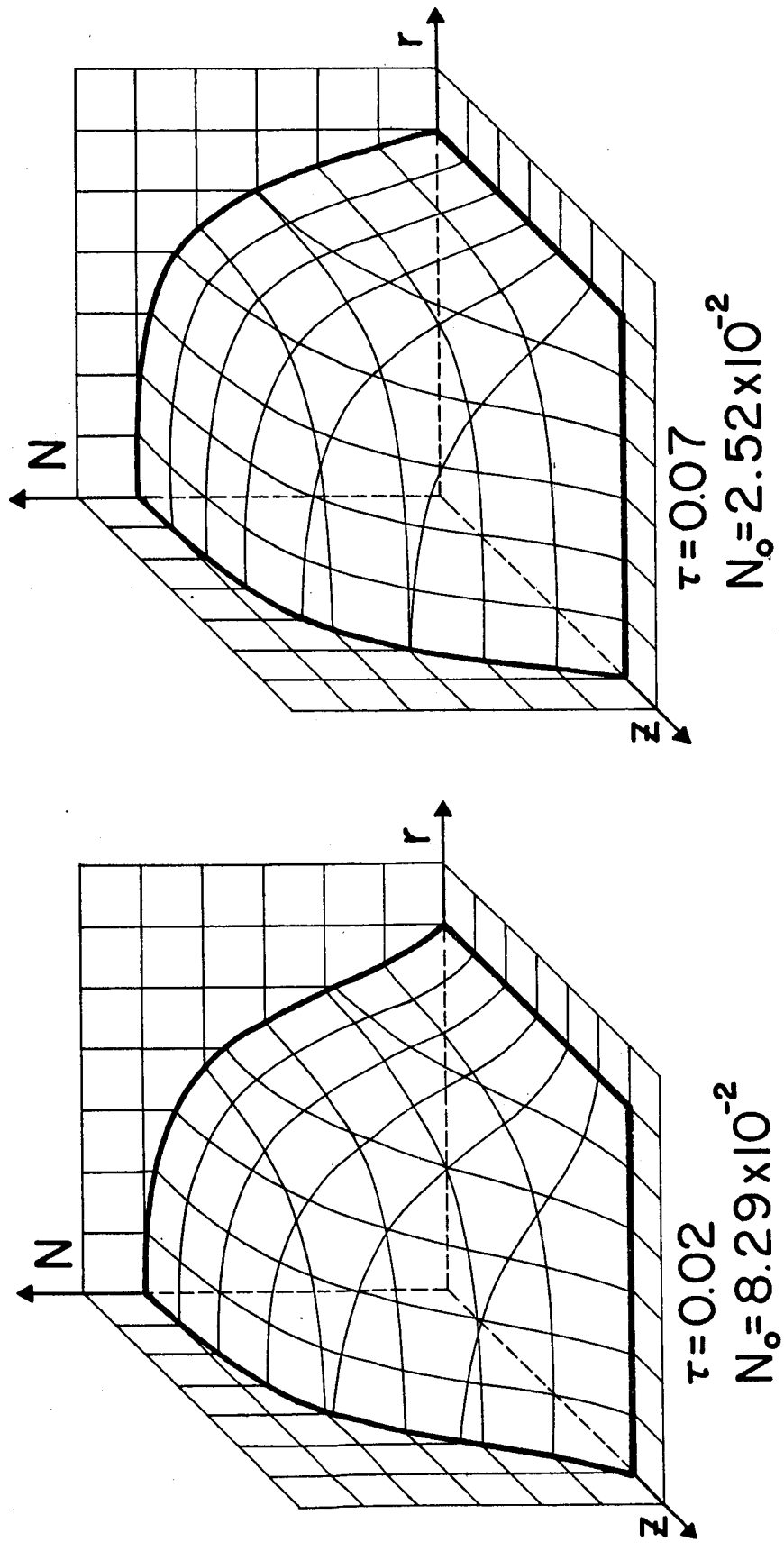

Figure

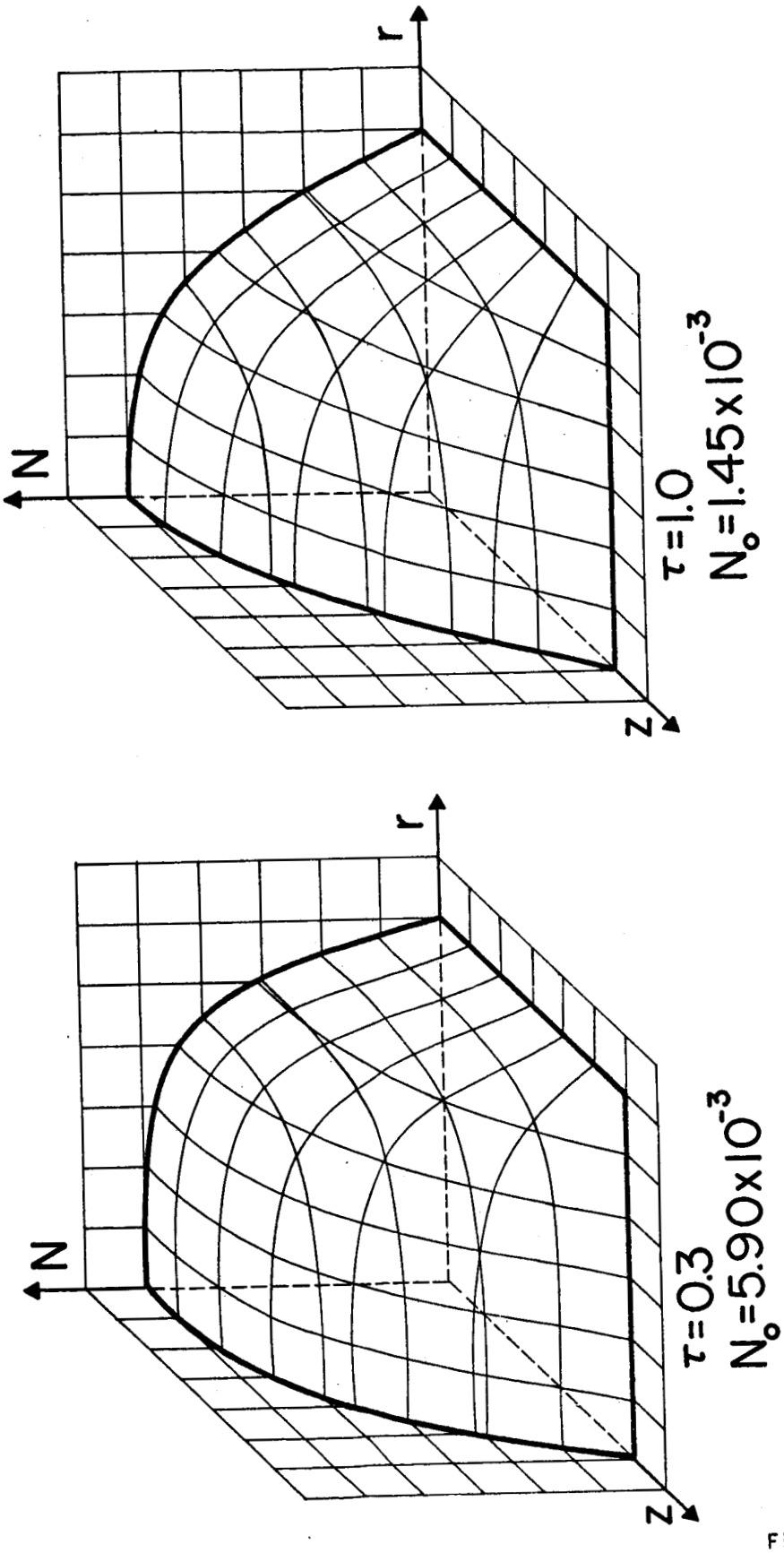

Figure 8C/3

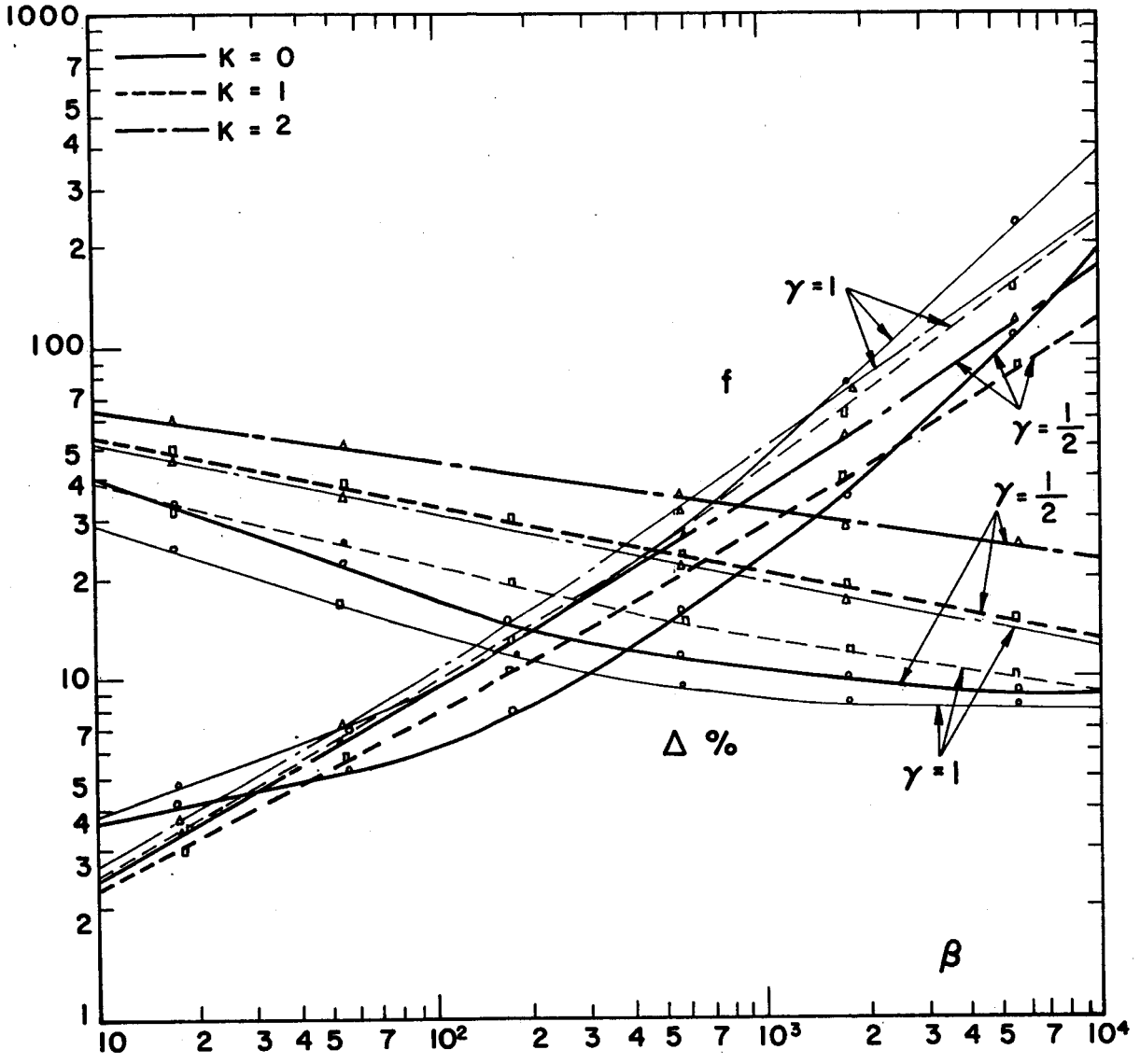
K = 0
K = 1
K = 2
γ = 1
γ = 1/2
γ = 1/2
γ = 1
f
Δ %
β
1000
7
5
4
3
2
100
7
5
4
3
2
10
7
5
4
3
2
1
10
2
3
4
5
7
10²
2
3
4
5
7
10³
2
3
4
5
7
10⁴

Figure 9a

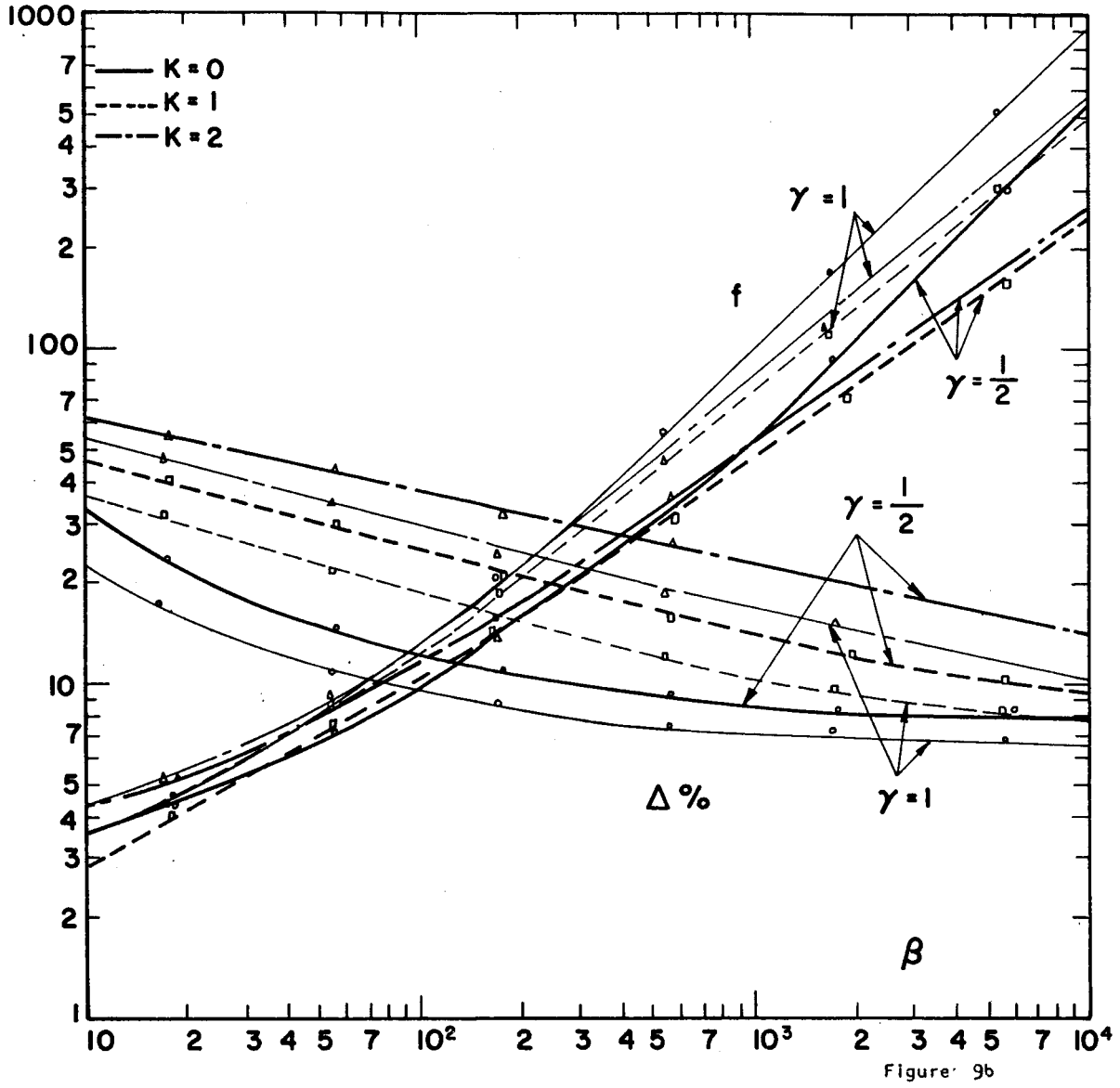
1000
7
5
4
3
2
100
7
5
4
3
2
10
7
5
4
3
2
1
K = 0
K = 1
K = 2
γ = 1
f
γ = 1/2
γ = 1/2
Δ %
γ = 1
β
10
2
3
4
5
7
10²
2
3
4
5
7
10³
2
3
4
5
7
10⁴

Figure 9b

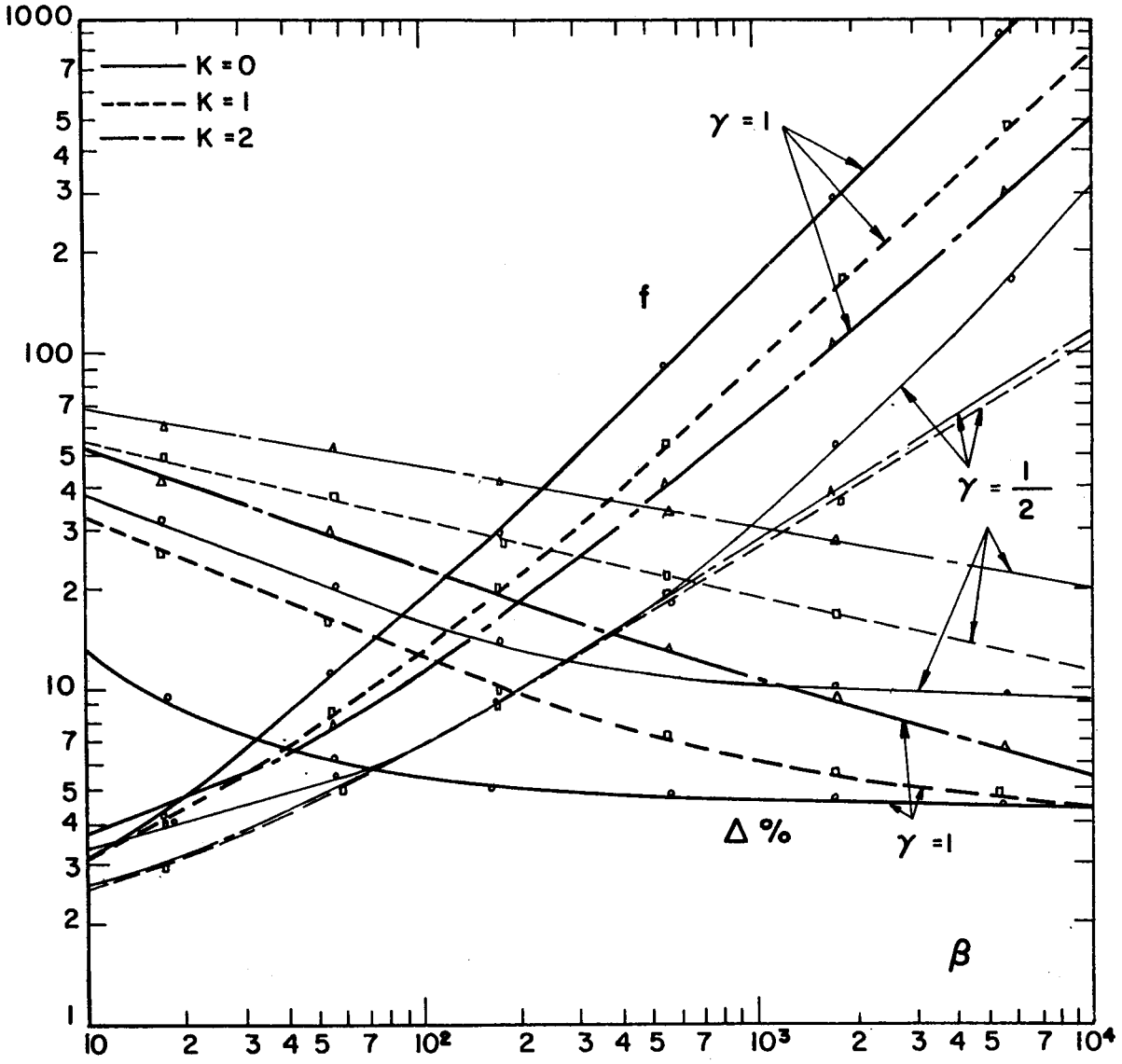
1000
7
5
4
3
2
100
7
5
4
3
2
10
7
5
4
3
2
1
K = 0
K = 1
K = 2
γ = 1
f
γ = 1/2
Δ %
γ = 1
β
10
2
3
4
5
7
10²
2
3
4
5
7
10³
2
3
4
5
7
10⁴

Figure 9c

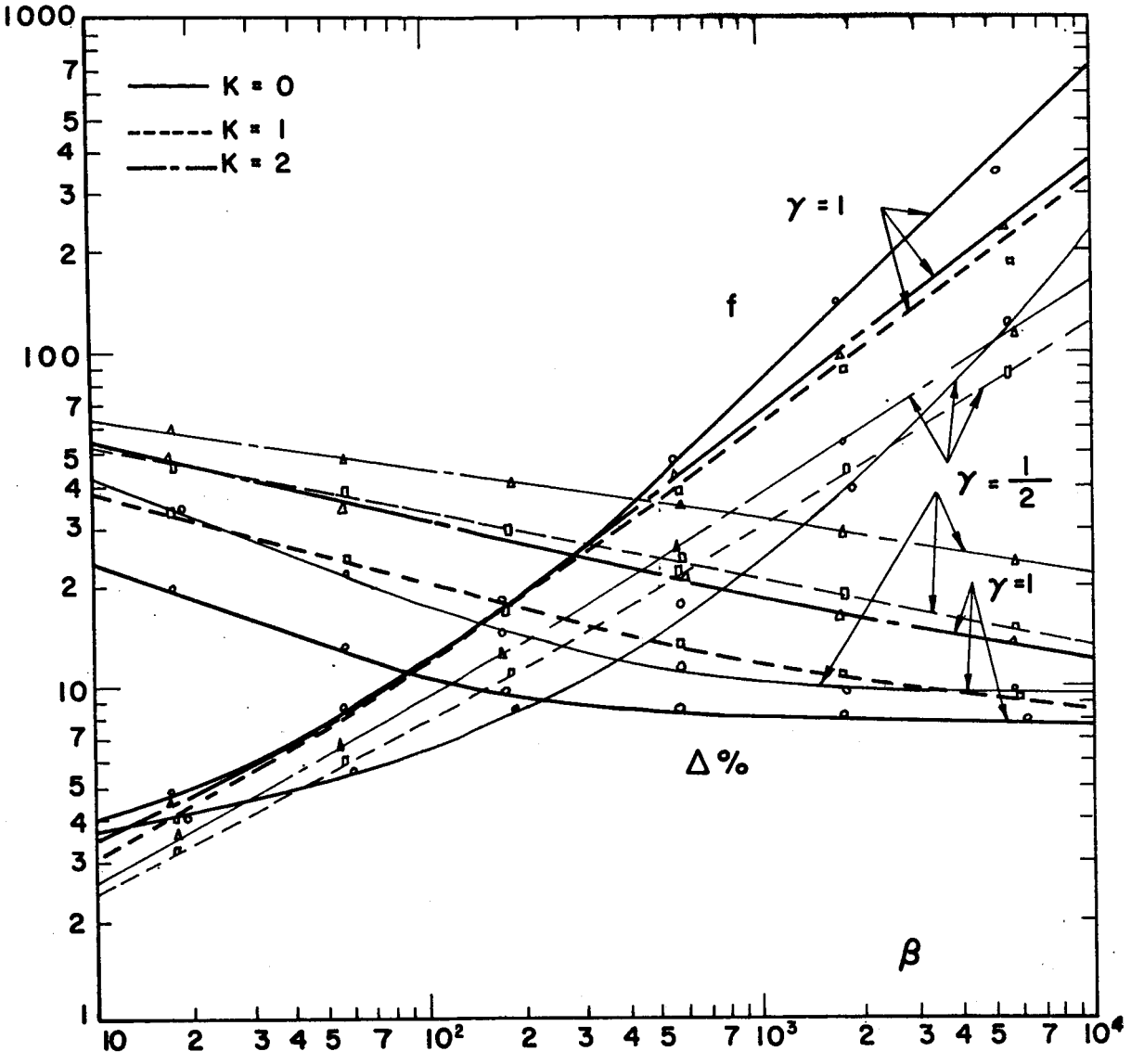
1000
7
5
4
3
2
100
7
5
4
3
2
10
7
5
4
3
2
1
K = 0
K = 1
K = 2
γ = 1
f
γ = 1/2
γ = 1
Δ %
β
10
2
3
4
5
7
10²
2
3
4
5
7
10³
2
3
4
5
7
10⁴

Figure 10a

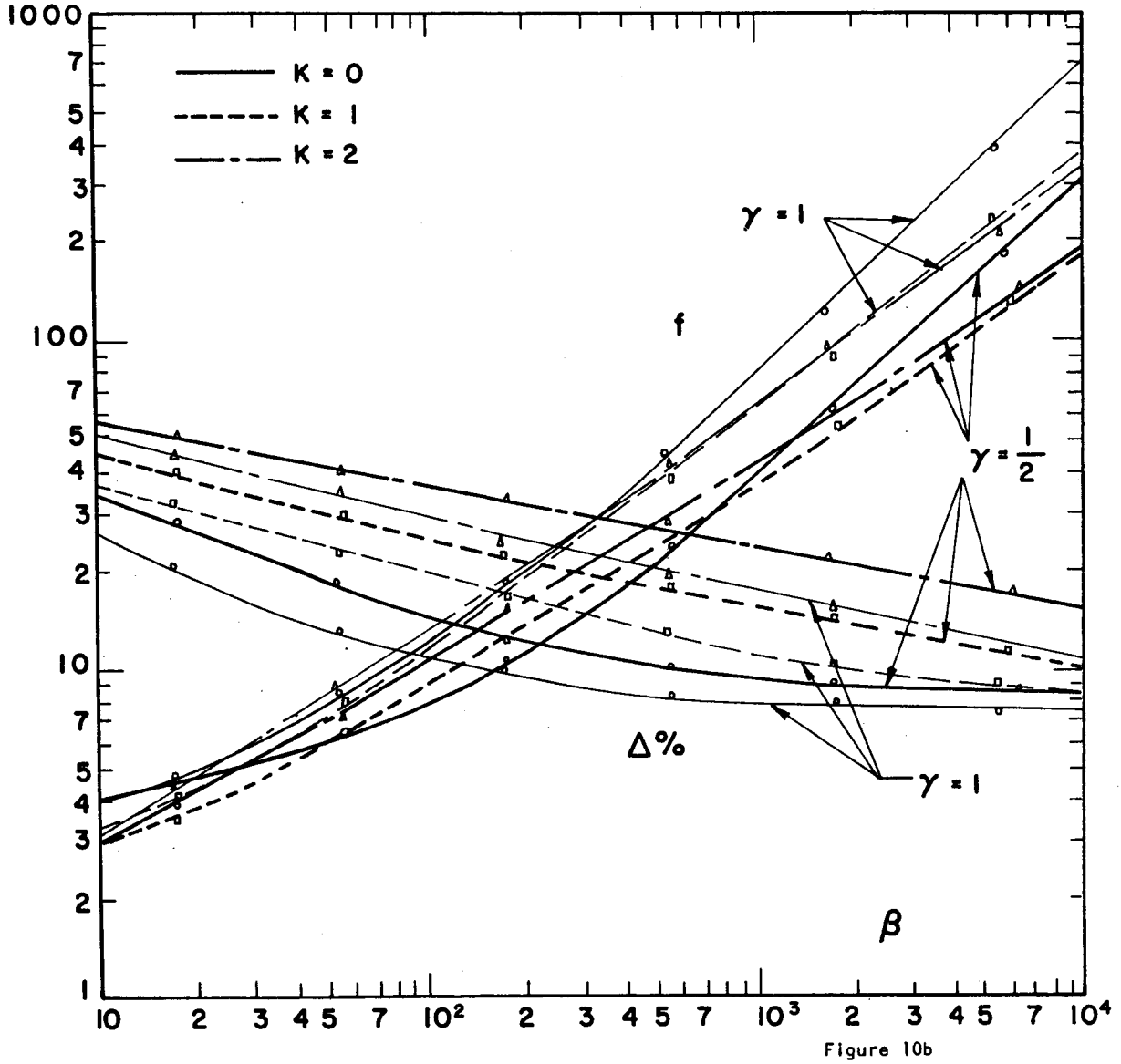
1000
7
5
4
3
2
100
7
5
4
3
2
10
7
5
4
3
2
1
10
2
3
4
5
7
10²
2
3
4
5
7
10³
2
3
4
5
7
10⁴
K = 0
K = 1
K = 2
γ = 1
f
γ = 1/2
Δ%
γ = 1
β

Figure 10b

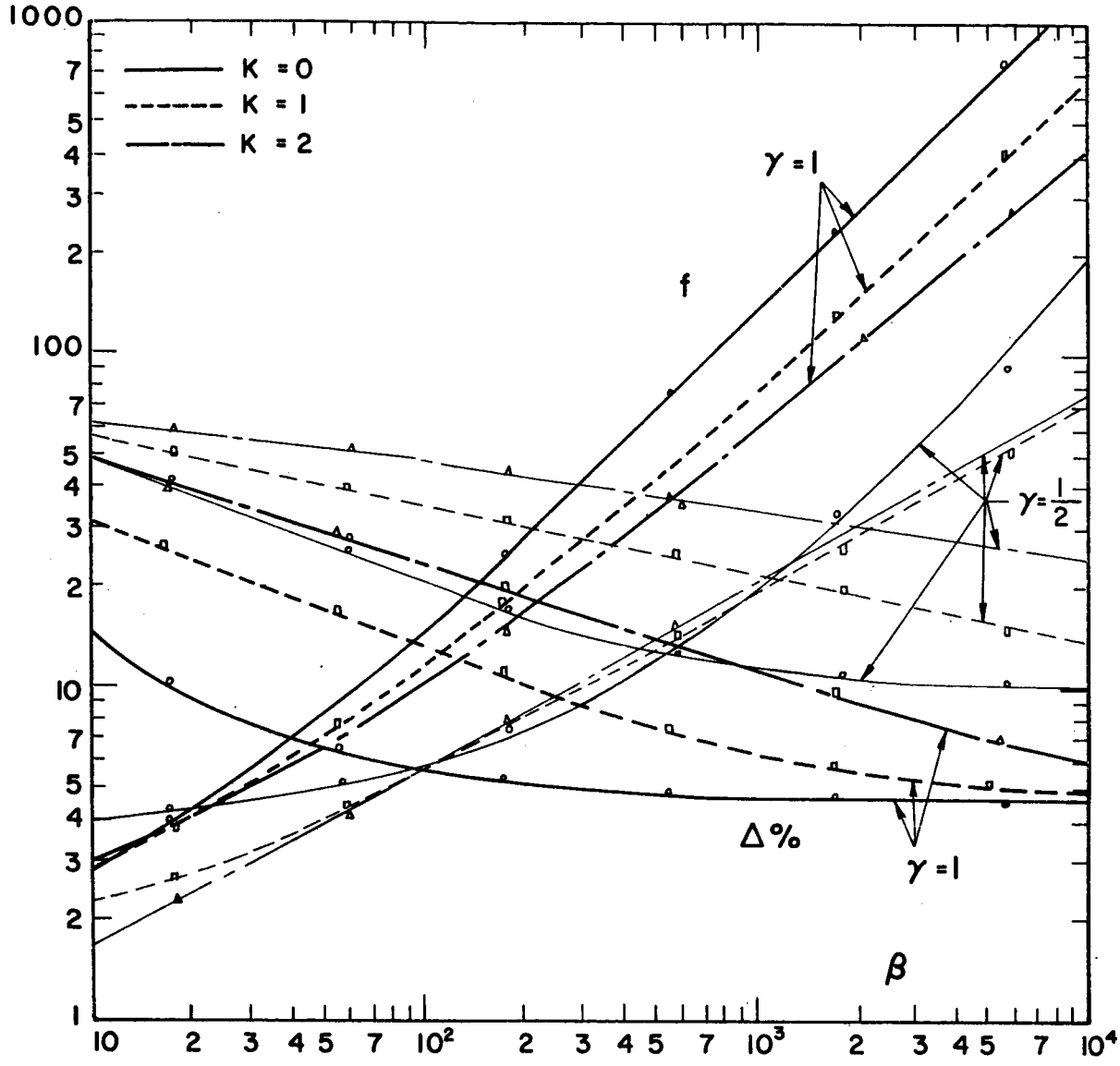
1000
7
5
4
3
2
100
7
5
4
3
2
10
7
5
4
3
2
1
K = 0
K = 1
K = 2
γ = 1
f
γ = 1/2
Δ%
γ = 1
β
10
2
3
4
5
7
10²
2
3
4
5
7
10³
2
3
4
5
7
10⁴

Figure 10c

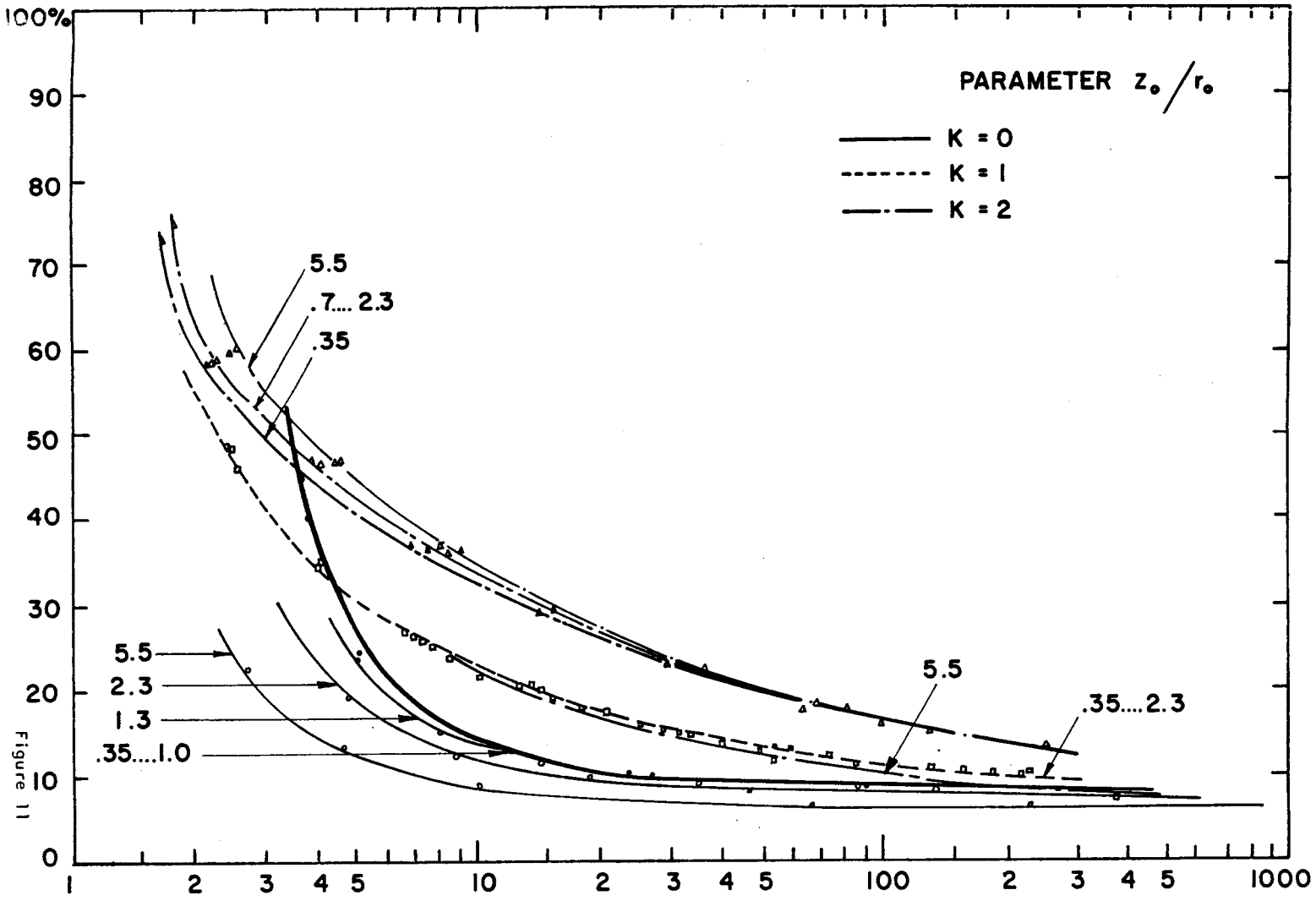
100%
90
80
70
60
50
40
30
20
10
0
1
2
3
4
5
10
2
3
4
5
100
2
3
4
5
1000
PARAMETER z_o/r_o
K = 0
K = 1
K = 2
5.5
.7.... 2.3
.35
5.5
2.3
1.3
.35....1.0
5.5
.35....2.3

Figure 11

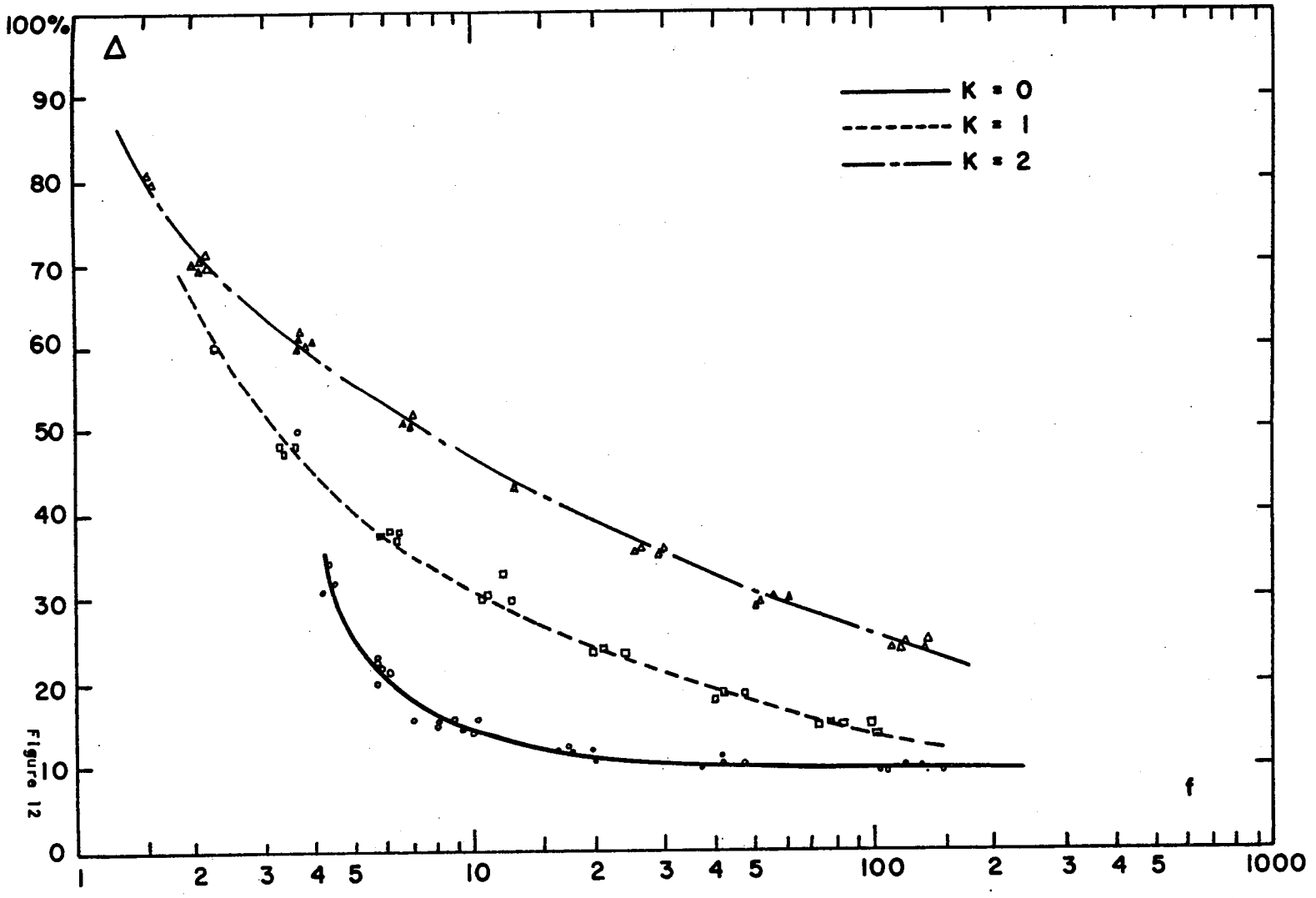
100%
90
80
70
60
50
40
30
20
10
0
Δ
K = 0
K = 1
K = 2
f
1
2
3
4
5
10
2
3
4
5
100
2
3
4
5
1000

Figure 12

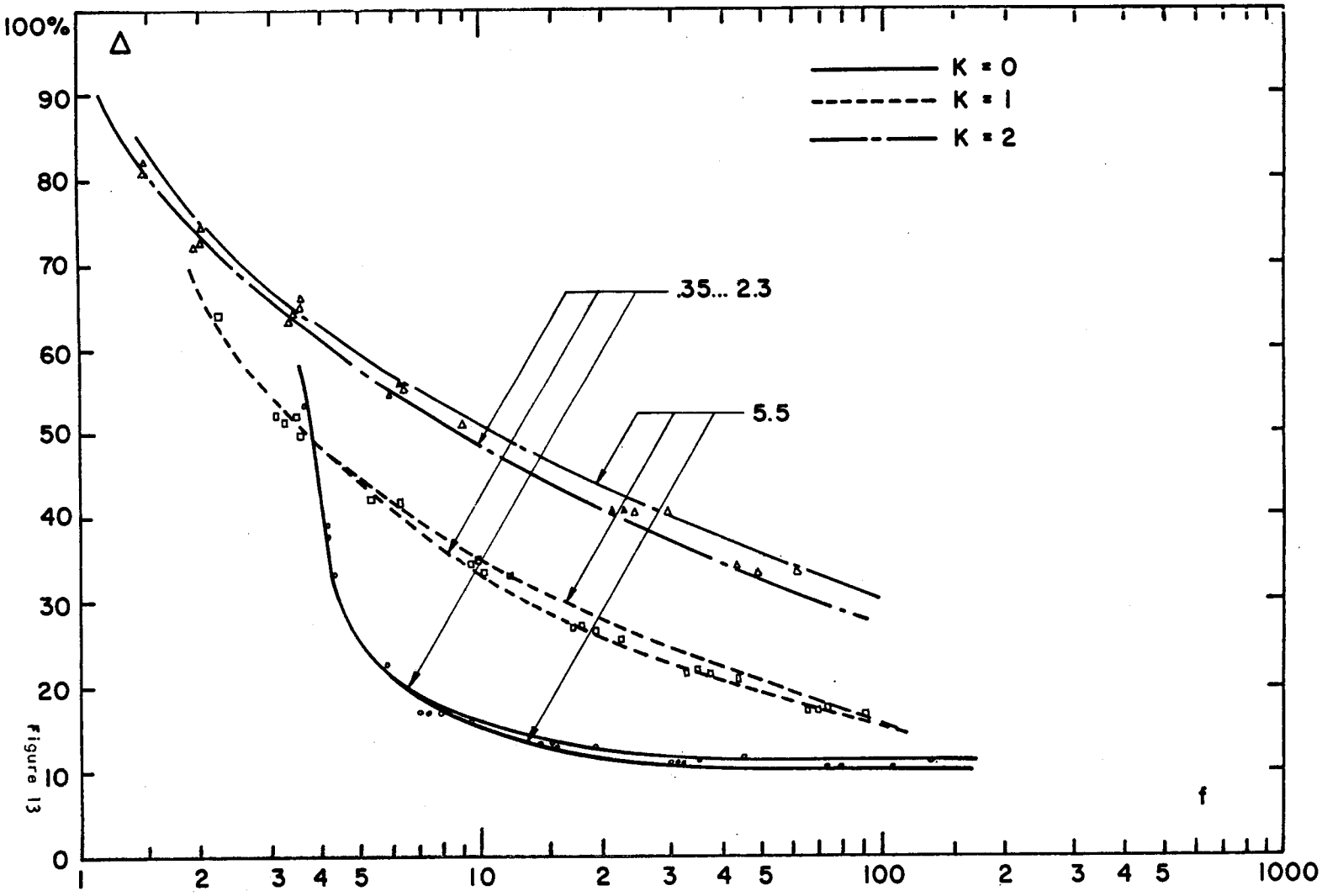
100%
90
80
70
60
50
40
30
20
10
0
Δ
K = 0
K = 1
K = 2
.35... 2.3
5.5
f
1
2
3
4
5
10
2
3
4
5
100
2
3
4
5
1000

Figure 13

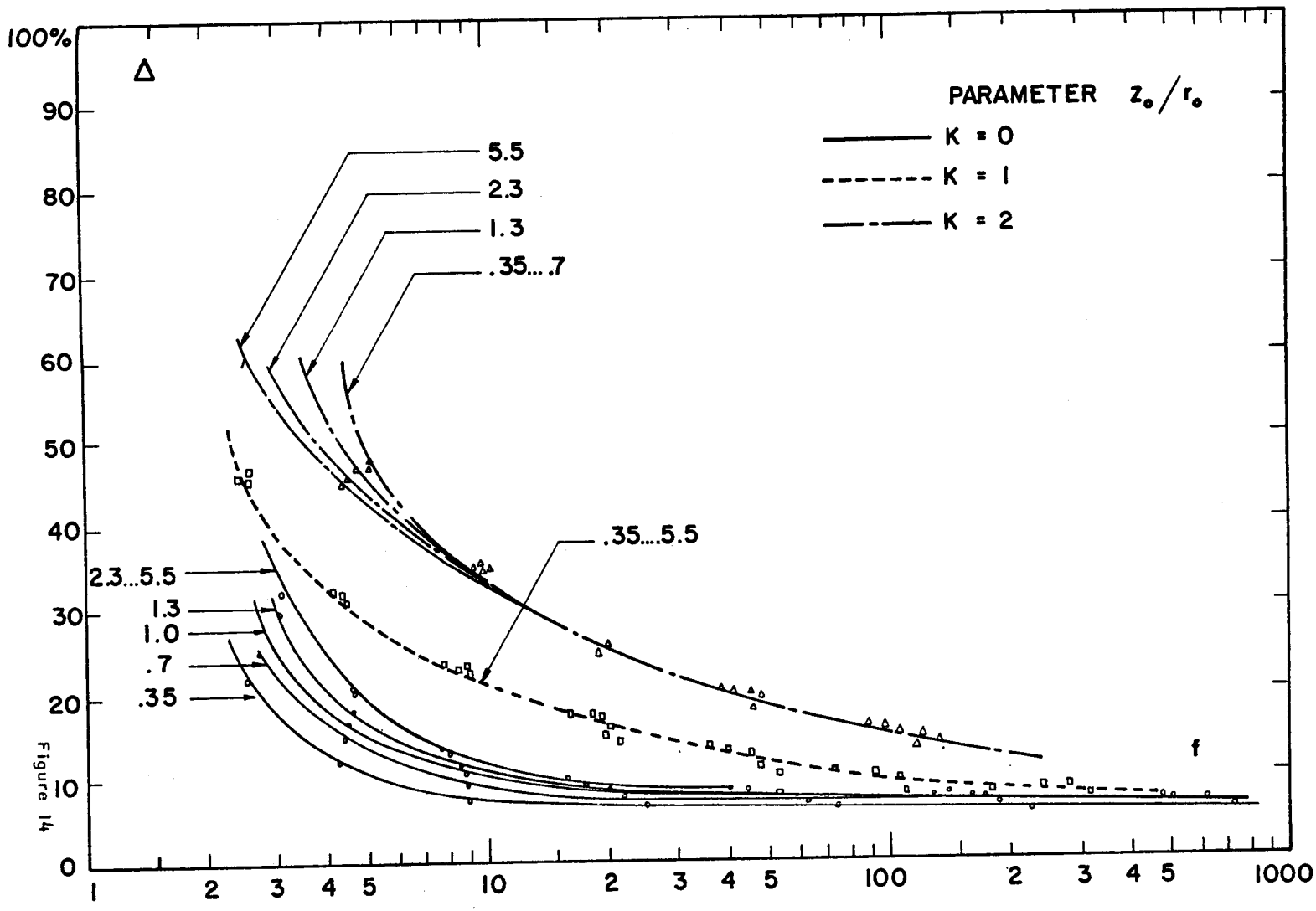
100%
90
80
70
60
50
40
30
20
10
0
Δ
PARAMETER z_o/r_o
K = 0
K = 1
K = 2
5.5
2.3
1.3
.35...7
.35...5.5
2.3...5.5
1.3
1.0
.7
.35
f
1
2
3
4
5
10
2
3
4
5
100
2
3
4
5
1000

Figure 14

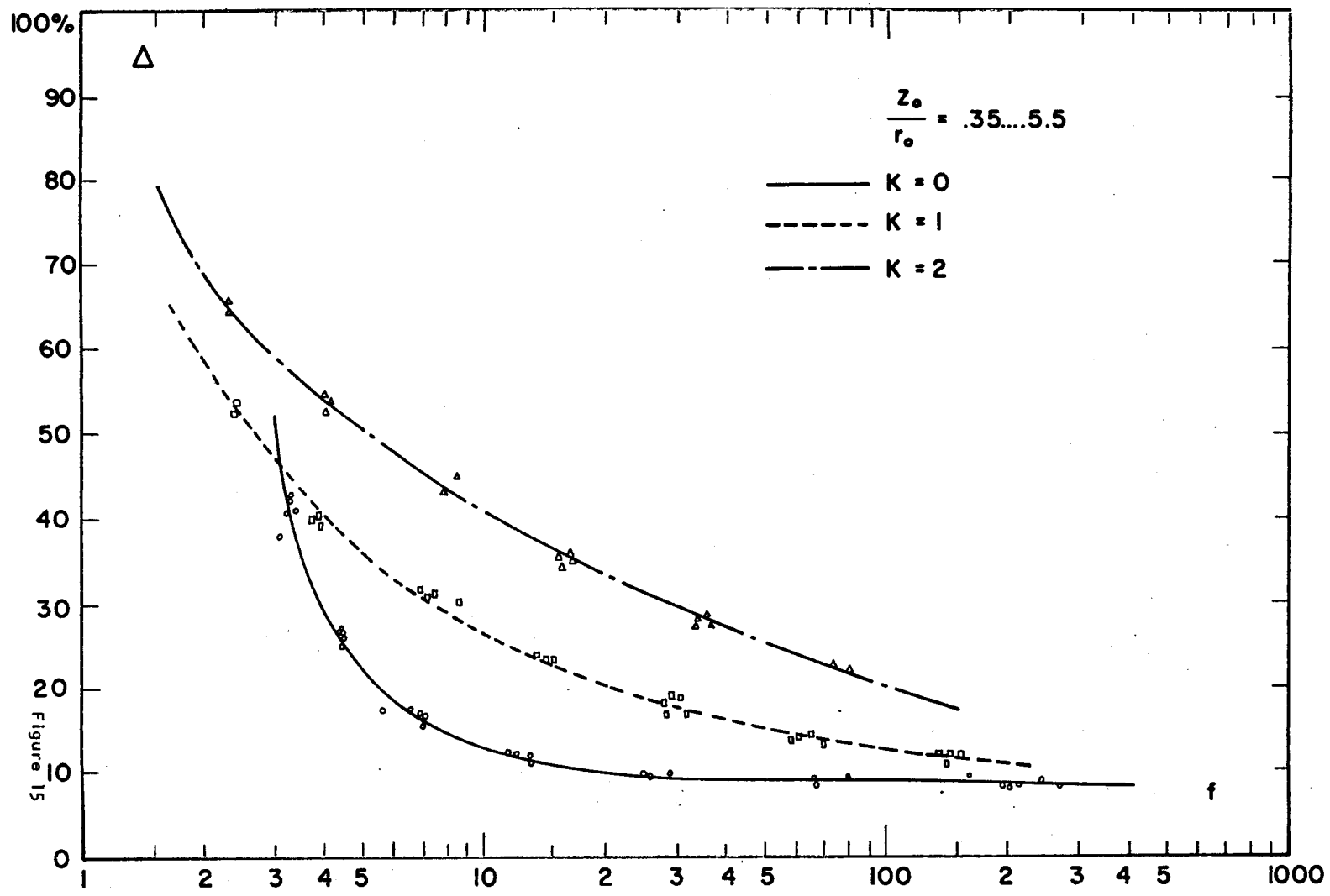
100%
90
80
70
60
50
40
30
20
10
0
Δ
$\frac{Z_o}{r_o}$ = .35....5.5
K = 0
K = 1
K = 2
1
2
3
4
5
10
2
3
4
5
100
2
3
4
5
1000
f

Figure 15

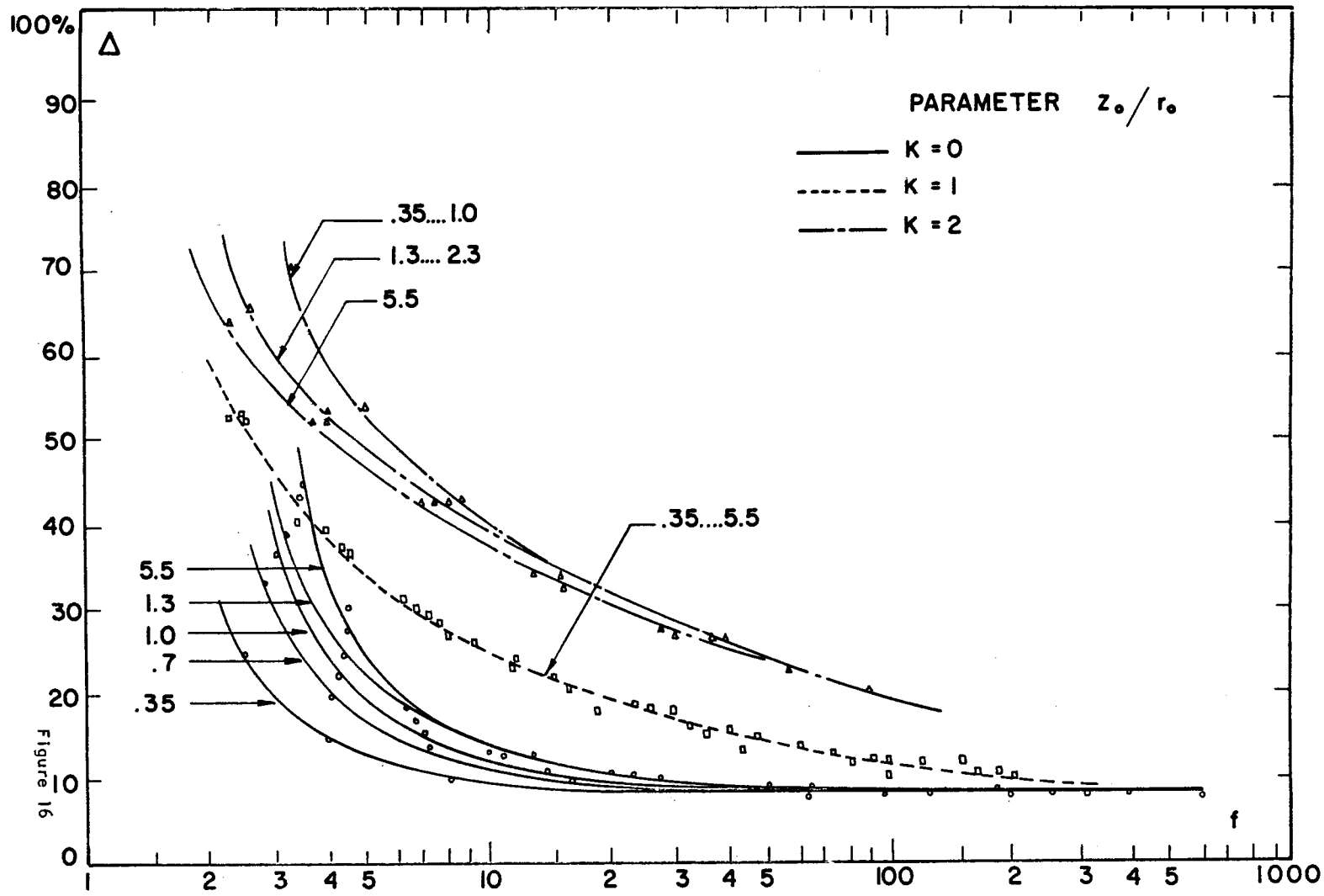
100%
Δ
90
80
70
60
50
40
30
20
10
0
PARAMETER z_o / r_o
K = 0
K = 1
K = 2
.35.... 1.0
1.3.... 2.3
5.5
.35....5.5
5.5
1.3
1.0
.7
.35
f
1
2
3
4
5
10
2
3
4
5
100
2
3
4
5
1000

Figure 16

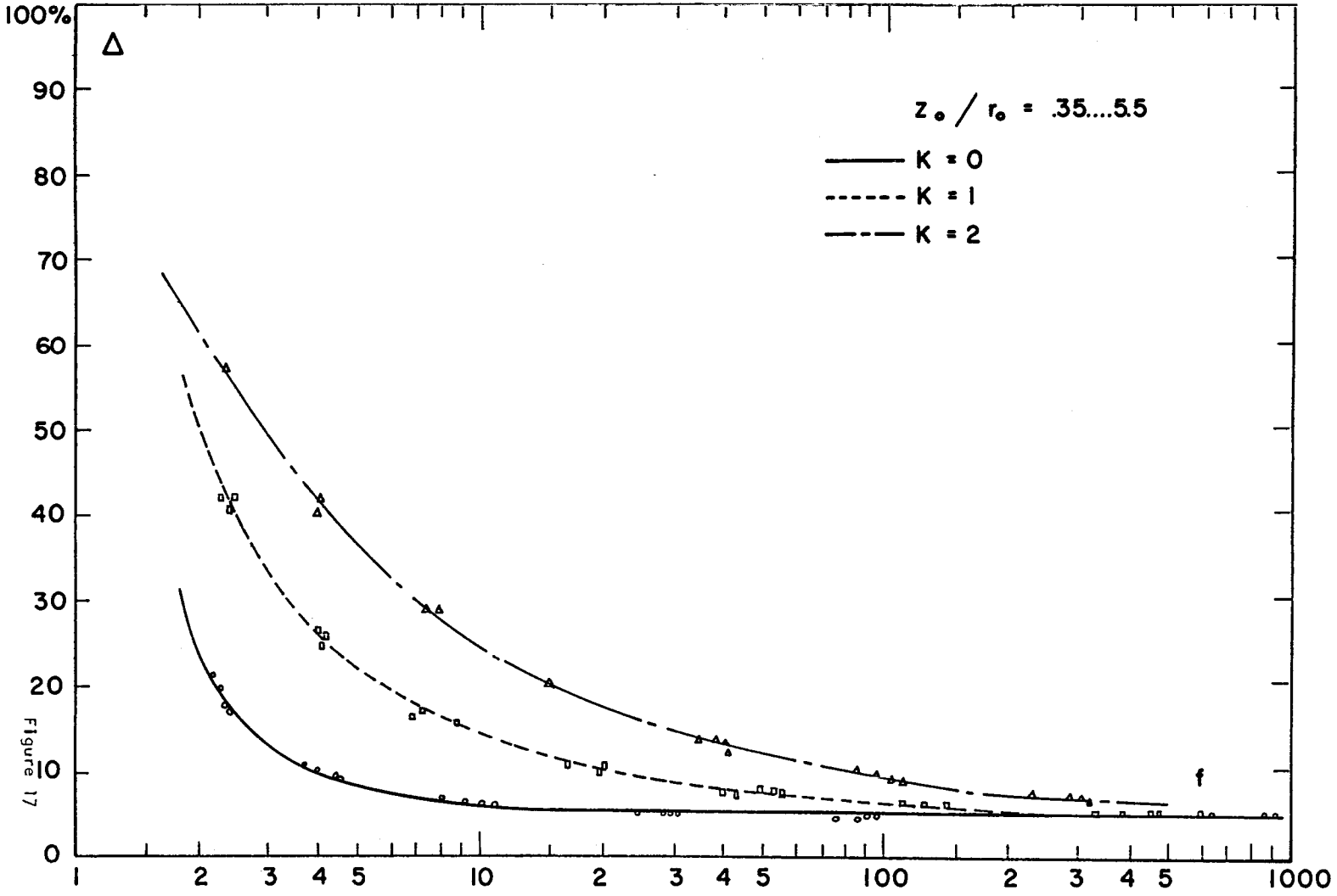
100%
90
80
70
60
50
40
30
20
10
0
Δ
z_o / r_o = .35....5.5
K = 0
K = 1
K = 2
f
1
2
3
4
5
10
2
3
4
5
100
2
3
4
5
1000

Figure 17

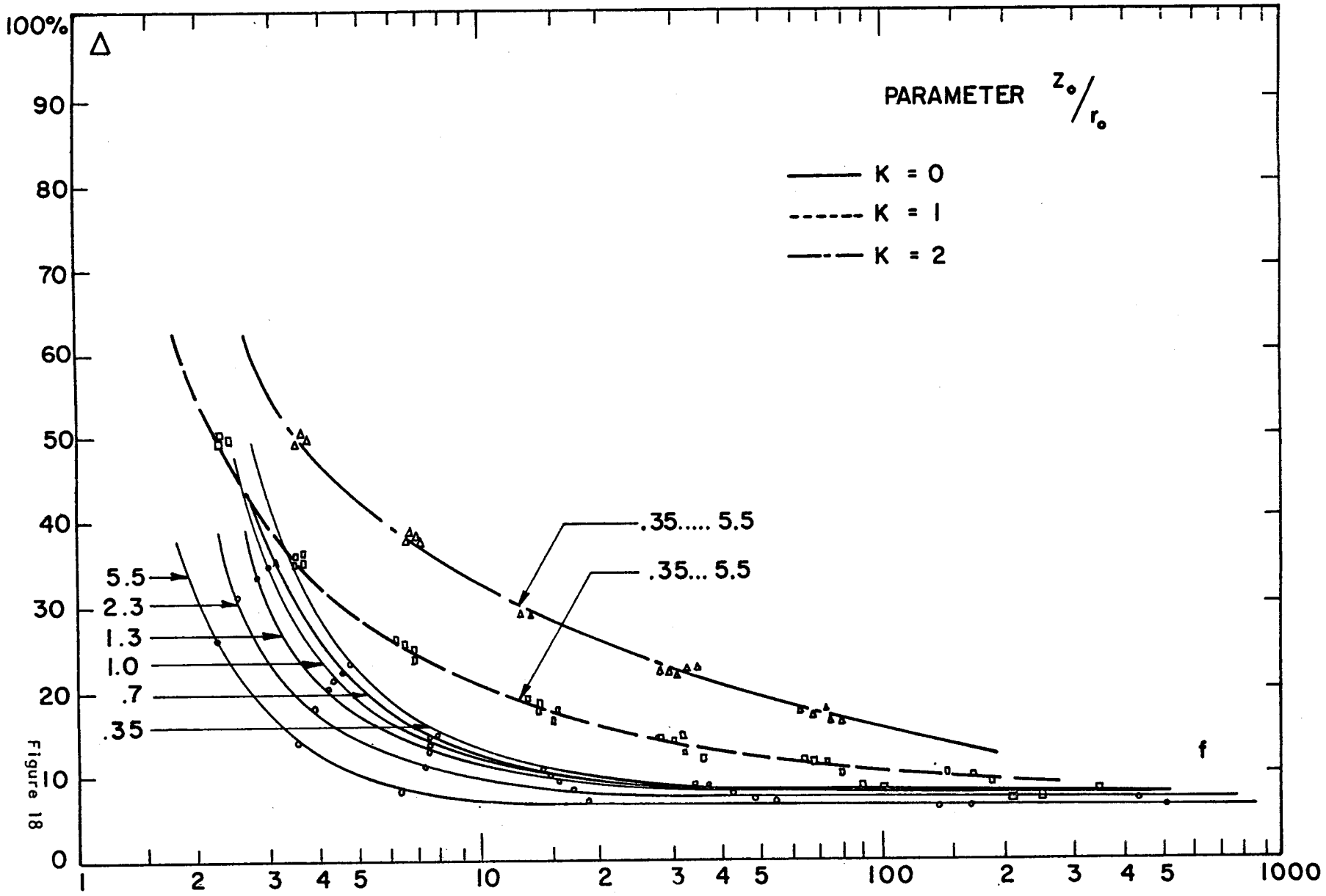
100%
Δ
90
80
70
60
50
40
30
20
10
0
PARAMETER z_o/r_o
K = 0
K = 1
K = 2
.35..... 5.5
.35... 5.5
5.5
2.3
1.3
1.0
.7
.35
f
1
2
3
4
5
10
2
3
4
5
100
2
3
4
5
1000

Figure 18

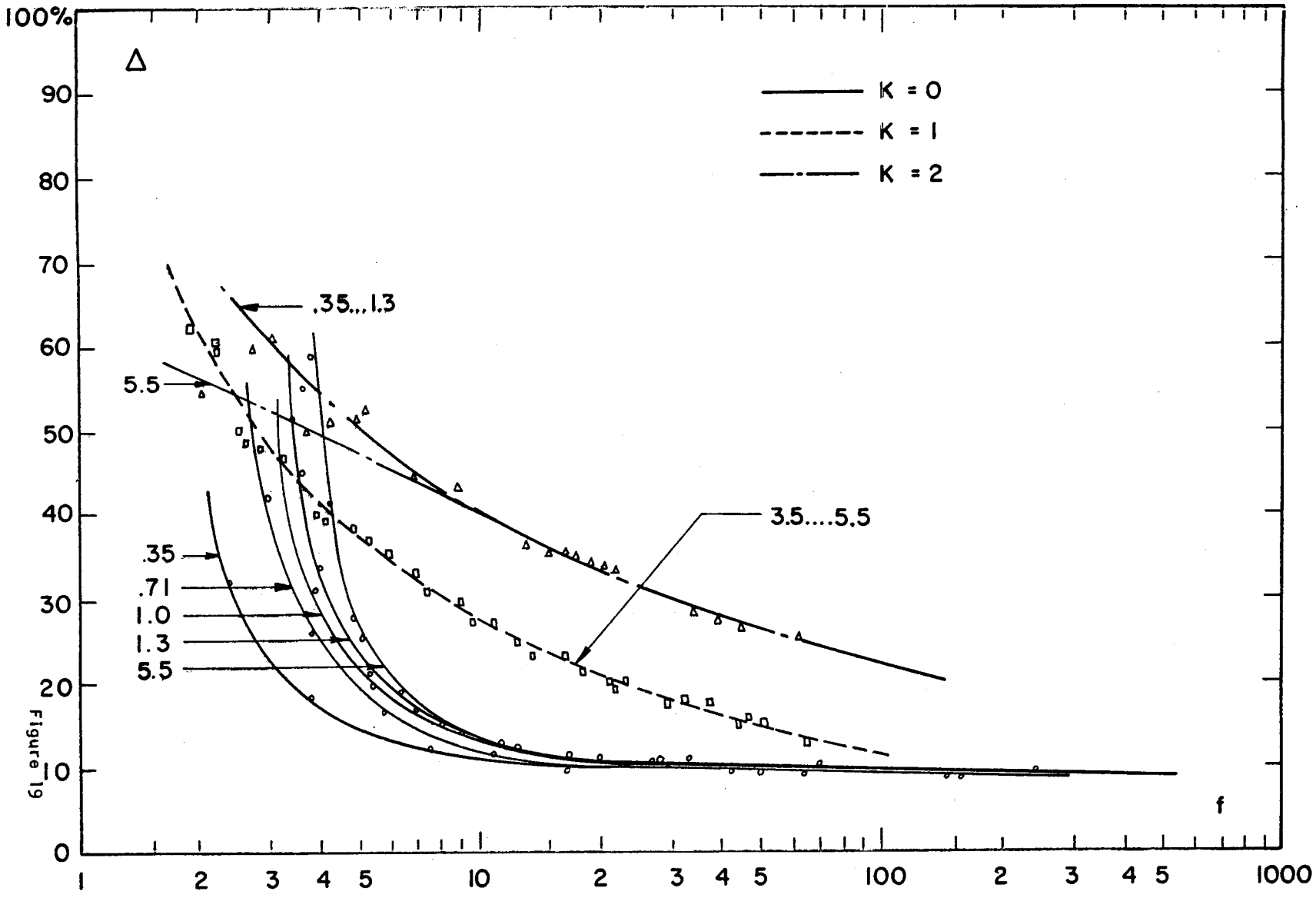
100%
90
80
70
60
50
40
30
20
10
0
Δ
K = 0
K = 1
K = 2
.35...1.3
5.5
3.5....5.5
.35
.71
1.0
1.3
5.5
f
1
2
3
4
5
10
2
3
4
5
100
2
3
4
5
1000

Figure 19

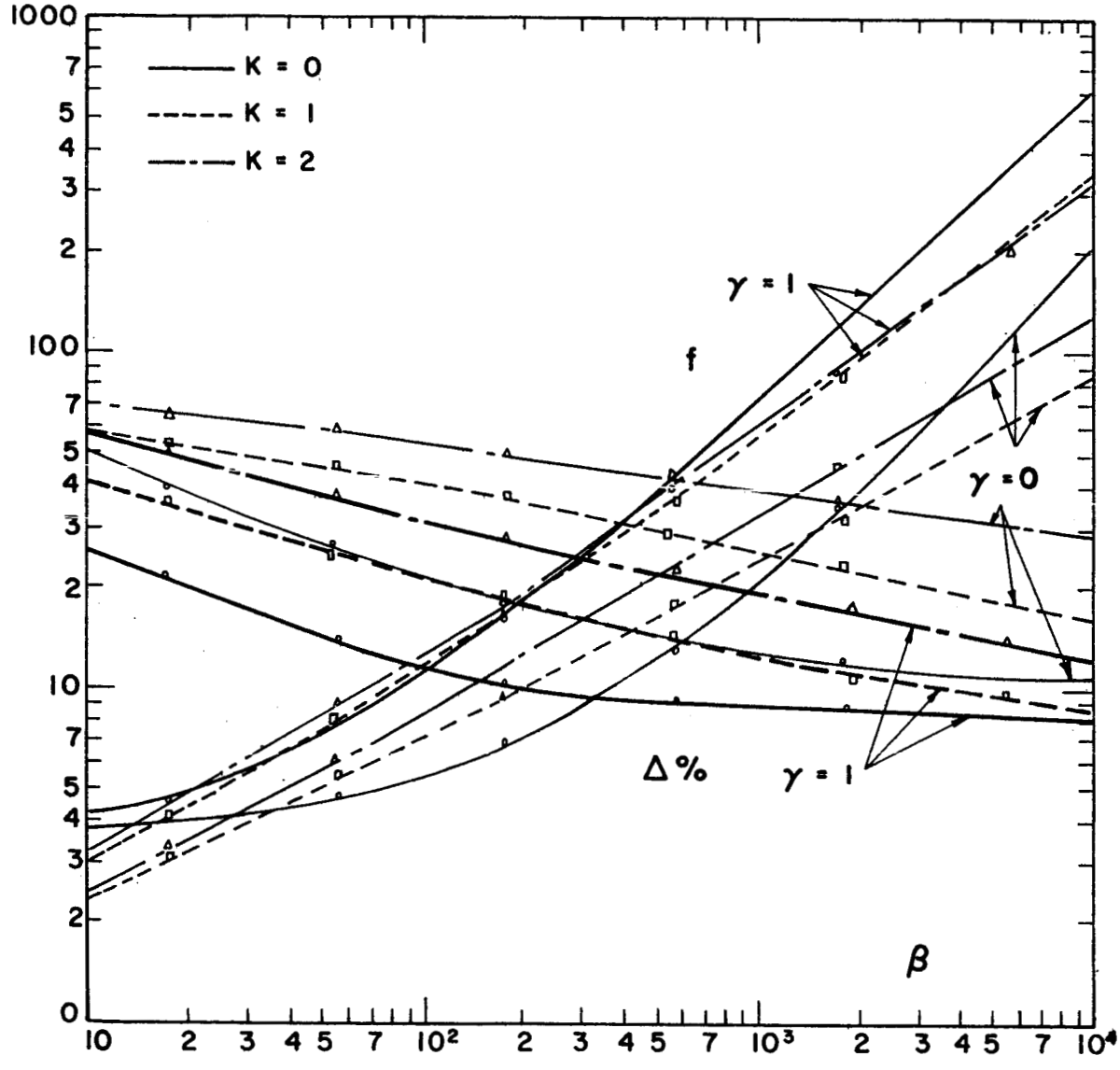
1000
7
5
4
3
2
100
7
5
4
3
2
10
7
5
4
3
2
0
K = 0
K = 1
K = 2
γ = 1
f
γ = 0
Δ%
γ = 1
β
10
2
3
4
5
7
10²
2
3
4
5
7
10³
2
3
4
5
7
10⁴

Figure 20

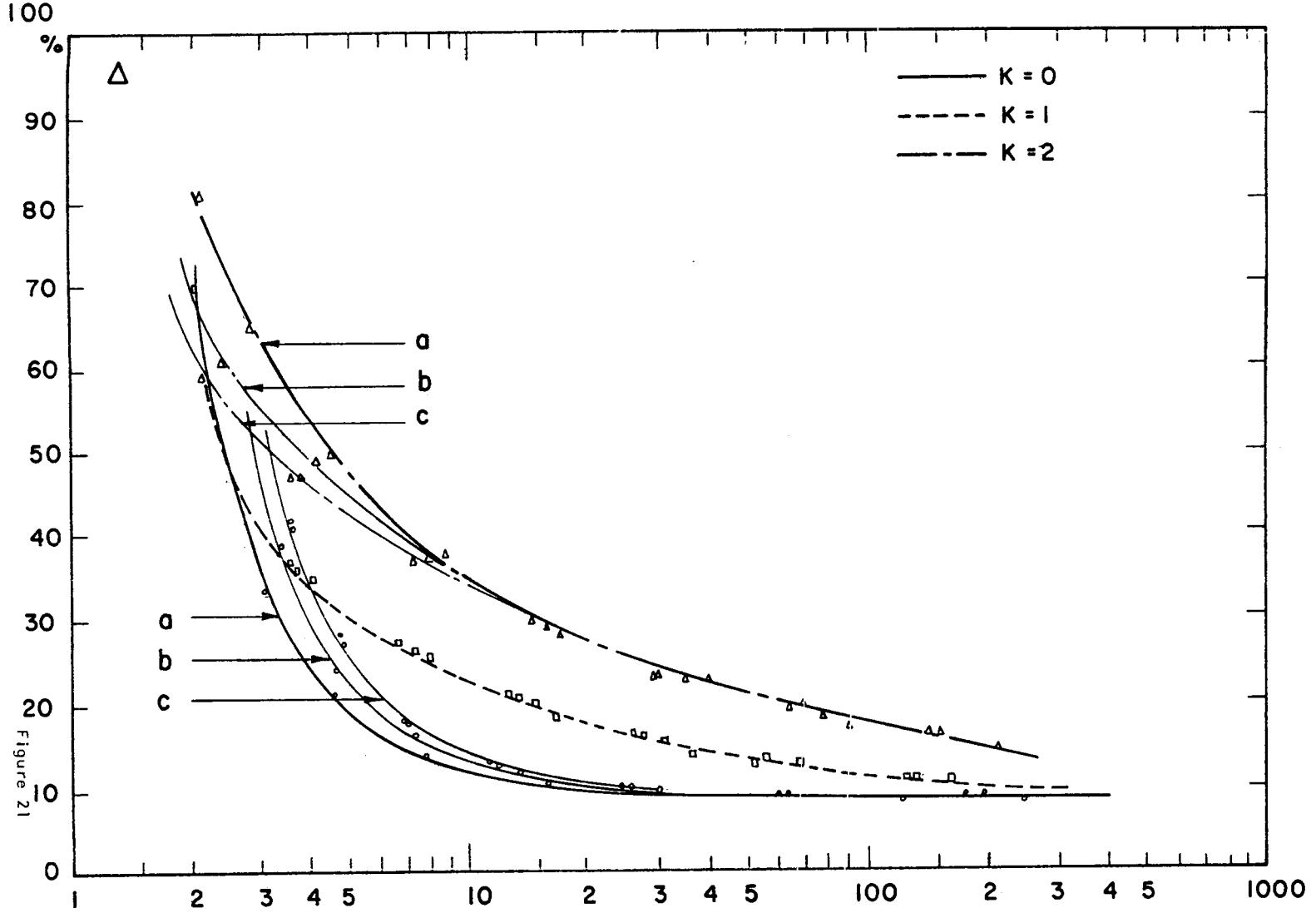
100
%
Δ
K = 0
K = 1
K = 2
90
80
70
60
50
40
30
20
10
0
a
b
c
a
b
c
1
2
3
4
5
10
2
3
4
5
100
2
3
4
5
1000

Figure 21

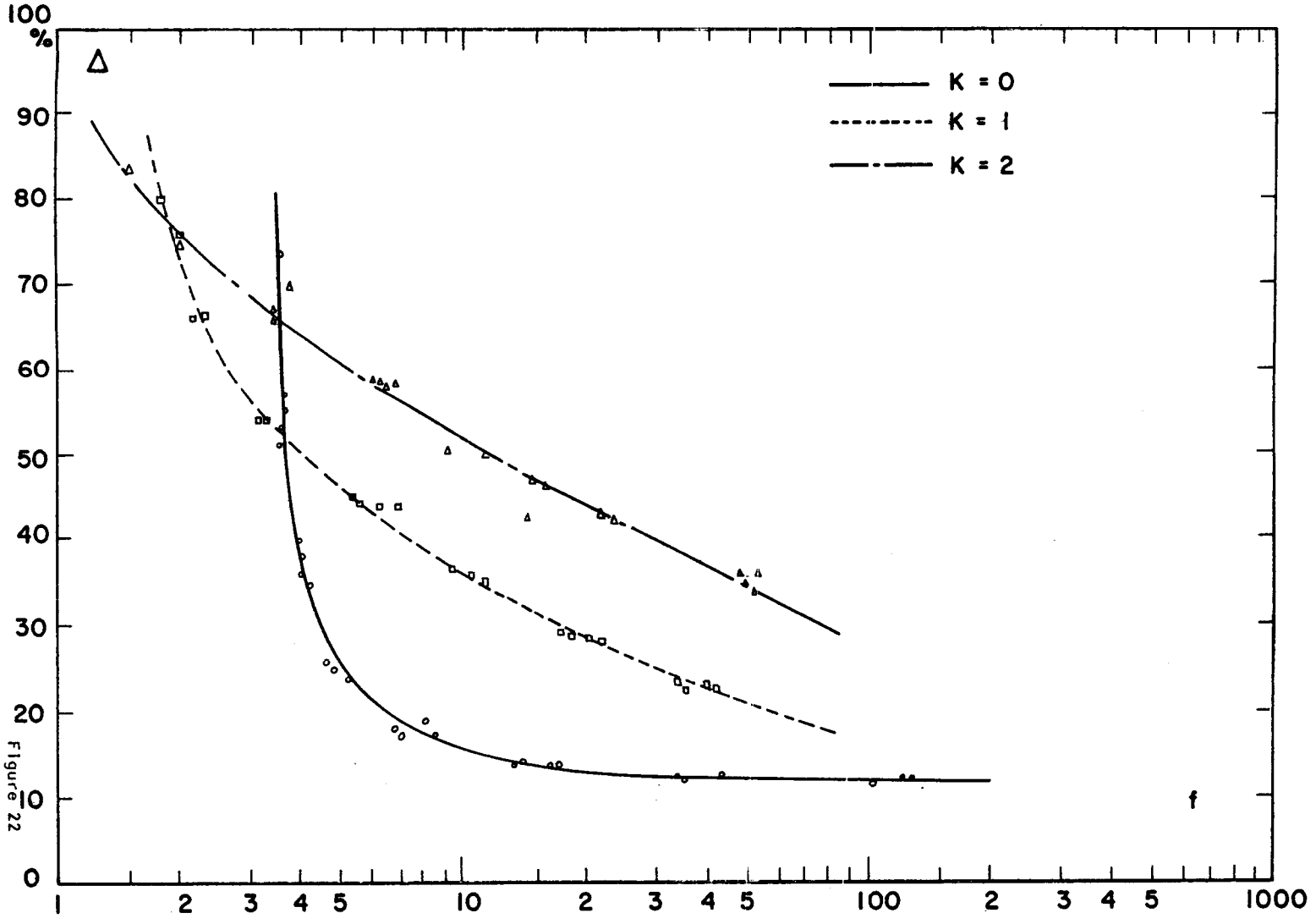
100
%
90
80
70
60
50
40
30
20
10
0
Δ
K = 0
K = 1
K = 2
f
1
2
3
4
5
10
2
3
4
5
100
2
3
4
5
1000

Figure 22